FACULDADE DE ENGENHARIA DA UNIVERSIDADE DO PORTO

Development of customized 3D structures for bone regeneration by Additive Manufacturing

Filipa Andreia Martins Leal

MSc in Bioengineering - Biomedical Engineering

Supervisor: José Domingos da Silva Santos, PhD

Co-Supervisor: Maria Ascensão Ferreira Silva Lopes, PhD

June 23, 2019

Development of customized 3D structures for bone regeneration by Additive Manufacturing

Filipa Andreia Martins Leal

MSc in Bioengineering - Biomedical Engineering

June 23, 2019

Resumo

Os enxertos ósseos são os segundos tecidos mais transplantados no mundo, sendo que o uso de substitutos ósseos em cirurgias tem vindo a aumentar a cada ano. Os mais utilizados são os aloenxertos e os autoenxertos, no entanto estes possuem várias desvantagens e deste modo têm vindo a ser produzidos enxertos sintéticos. Uma área que tem vindo a ser investigada é a produção de substitutos ósseos através do fabrico aditivo de cerâmicos, uma vez que estas técnicas conseguem produzir geometrias complexas e escaláveis, possuindo ainda capacidade de controlo da localização, interconectividade e geometria de poros permitindo a produção de substitutos ósseos com propriedades semelhantes às do osso.

Nesta dissertação foi realizada a otimização de um procedimento promissor de forma a produzir enxertos ósseos sintéticos impressos em 3D, com alto conteúdo em sólidos e capaz de mimetizar a arquitetura porosa e complexa do osso humano.

Através de uma tomografia computadorizada é criado um modelo CAD com a microestrutura e macroestrutura exata do osso natural, que depois é impresso através de uma impressora DLP.

Isto requereu a otimização dos parâmetros de impressão visto que estes são de extrema importância nas propriedades finais do excerto.

Quatro pós de hidroxiapatite com origens diferentes (HA1, HA2, HA3 e HA4) foram analisados com o intuito de avaliar as suas influências na viscosidade das suspensões. Desta forma diversas formulações foram criadas com concentrações de hidroxiapatite entre 35.0 m/v% e 50.0 m/v% e com concentrações de surfactante entre 0.5 m/m% e 2.0 m/m% de forma a obter um equilibrio entre alta concentração de sólidos e baixa viscosidade da suspensão.

Após o término da impressão, as peças necessitam de ser imersas num solvente que assegure que a resina não polimerizada seja removida sem criar fissuras e delaminações. Foi então estudada a influência dos solventes S1, S2 e S3 na formação de fissuras e delaminações nas peças impressas em 3D.

As impressões foram bem sucedidas utilizando o pó HA1 e HA3 no entanto, concentrações de sólidos de 50.0 m/v% apenas foram atingidas com formulações constituídas pelo pó HA3. Menores valores de viscosidade foram obtidos com a adição de 0.5 m/m% de surfactante, e todas as formulações apresentaram viscosidades inferiores 3 $Pa{\cdot}s$ a uma taxa de cisalhamento de 100 s^{-1}. As peças impressas em 3D apresentaram menor quantidade de fissuras e delaminações quando mergulhadas em S2, mas estudos posteriores devem ser realizados. Estas peças foram sujeitas a um tratamento térmico com dois estágios, um dos quais permite a combustão completa da resina e o outro permite a sinterização do pó, melhorando as propriedades mecânicas das peças impressas. Após sinterização do pó HA3, ocorreu uma pequena transformação de fase em β-TCP, que não é possível quantificar através da análise XRD.

Peças impressas em 3D com arquitetura semelhante ao osso trabecular foram obtidas a partir de formulações com 50.0 m/v% de sólidos, apresentando baixo número de fissuras visíveis e delaminação insignificante.

Abstract

Bone grafts are the second most transplanted tissue in the world, and the use of bone substitutes in surgeries has been increasing every year. The most commonly used bone grafts are allografts and autografts, however these show several drawbacks and, in this way, synthetic grafts have been produced. One area that has been investigated is the production of bone substitutes through the additive manufacture of ceramics since these techniques can produce complex and scalable geometries, also having the capacity of controlling the location, interconnectivity and the pore geometry allowing the production of bone substitutes with properties similar to those of human bone.

In this dissertation an optimization of a promising procedure was developed in order to produce a 3D printed synthetic bone graft with high solid content and able to reproduce the porous and complex bone architecture.

From a bone CT scan, a CAD model is created with the exact microstructure and macrostructure of the natural bone and then printed through a DLP printer. This required the optimization of the printing parameters since these are of extreme importance in the final properties of the graft.

Four hydroxyapatite powders of different origins (HA1, HA2, HA3 and HA4) were analysed in order to evaluate their influence on the viscosity of the suspensions. In this way various formulations were created with concentrations of hydroxyapatite between 35.0 w/v% and 50.0 w/v% and with surfactant concentrations between 0.5 wt% and 2.0 wt% in order to achieve a balance between high solids concentration and low viscosity of the suspension.

Upon completion of the printing, the parts need to be immersed in a solvent which ensures that the unpolymerized resin is removed without creating cracks and delamination. The influence of the solvents S1, S2 and S3 on the formation of cracks and delamination in 3D printed parts was then also studied.

3D printings were successful using the HA1 and HA3 powder however, solids concentrations of 50.0 w/v% were only reached with formulations constituted by HA3 powder. Lower viscosity values were obtained with the addition of 0.5 wt% of surfactant, and all formulations had lower viscosities than 3 $Pa{\cdot}s$ at a shear rate of 100 s^{-1}. The 3D printed pieces showed smaller number of cracks and delaminations when immersed in S2, but further studies should be carried out to completely eliminate such cracks. These pieces were subjected to a heating treatment with two stages, one of which allows the complete combustion of the resin and the other allows the final sintering of the powder, improving the mechanical properties of the printed parts. After sintering of the HA3 powder, a small phase transformation occurred in β-TCP, which can not be quantified by XRD analysis.

3D printed pieces with a porous architecture similar to trabecular bone were achieved from formulations with 50 wt% of solids, with low number of visible cracks and insignificant delamination.

Agradecimentos

Após cinco anos de desafios constantes, tristezas, alegrias, vitórias e derrotas, apenas posso agradecer a todos aqueles que me apoiaram e me deram força.

Em primeiro lugar, agradeço aos meus orientadores, Professor Doutor José Domingos Santos e Professora Doutora Maria Ascensão Lopes, pelo interesse, apoio e orientação prestada durante a realização desta dissertação.

À empresa parceira pela disponibilidade, prestabilidade e confiança depositada.

Às minhas amigas do F201, principalmente à Ana Azevedo, pelas gargalhadas, boa disposição, solidariedade, incentivo e pela paciência demonstrada nos momentos mais difíceis.

Aos meninos de Lisboa *grazie* por tornarem o Erasmus uma experiência memorável, pelos jantares e por todos os momentos, dos mais insólitos aos mais divertidos.

Aos meus melhores amigos, Joana Almeida Dias, Gabriel Lopes e Kinho, pelas palavras amigas, pelas risadas, pelas tardes de estudo, por me cativarem, encorajarem e pela paciência que demonstraram durante todos estes anos.

Às meninas da Araucária que decidiram acolher-me no primeiro ano da faculdade e nunca mais me largaram.

Às de sempre, Ana Lírio e Lucília Silva, por acreditarem em mim, pelo carinho, pelos cafés e tardes de galhofa.

E por último, aos meus pais, irmãos e avó Mila pela educação, esforço, amor, compreensão e generosidade. Sem eles, tudo isto seria impossível.

Filipa Leal

"To succeed in life, you need three things:
a wishbone, a backbone and a funny bone."

Reba McEntire

Contents

List of Figures

List of Tables

Abbreviations

3D	Three Dimensional
3DP	Three-Dimensional Printing
AM	Additive Manufacturing
ASTM	American Society for Testing and Materials
CAD	Computer Aided Design
CAGR	Compound Annual Growth Rate
CaP	Calcium Phosphate
CLI	Common Layer Interface
CT	Computed Tomography
DED	Direct Energy Deposition
DLP	Digital Light Processing
ECM	Extracellular Matrix
FEP	Fluorinated Ethylene Propylene
HA	Hydroxyapatite
HPGL	Hewlett-Packard Graphics Language
IGES	Initial Graphics Exchange Specifications
LCD	Liquid Crystal Display
LOM	Laminated Object Manufacturing
RP	Rapid Prototyping
SEM	Scanning Electron Microscopy
SLA	Stereolithography
STL	Standard Triangle Language
SLC	Stereolithography Contour
SLI	Spline File
TCP	Tricalcium Phosphate
USB	Universal Serial Bus
UV	Ultraviolet
XRD	X-ray Diffraction

Chapter 1

Introduction

Bone is a living and active tissue that support the body structurally, protect the vital organs, allow us to move, provide an environment for bone marrow where the blood cells are created, and they act as a storage area for minerals. This tissue is vascularized and is made of living cells that allow the bone to grow and to repair himself [1]. However, in the case of large-scale bone loss resultant from tumour resections and high impact trauma, the body cannot completely heal the bone defect without intervention because the injury is beyond the critical size [2]. The intervention is made through the replacement of the missing bone by a bone graft however, in the case of natural bone grafts can lead to pain, swelling, nerve injury, rejection of the bone graft, inflammation, reabsorption of the graft and the graft may not fit perfectly [3]. More than two millions bone grafting surgeries are performed every year [4] and in 2016 the bone grafts and substitutes market size was evaluated at USD 2.4 billion and it is expected to grow in the next years at a compound annual growth rate (CAGR) of 5.5%. The prevalence of orthopedic diseases has increased over the years becoming increasingly necessary the adoption of bone grafts. The market is divided in natural and synthetic materials, as can be seen in Figure 1.1. It is likely that the growth of natural bone grafts will be limited due to lack of availability, in the case of autografts, and in the case of allografts due to transmission of diseases and viruses. Synthetic bone grafts have gained popularity and consequently is estimated to grow in the forecasting years since it suppresses the problems mentioned above [5]. These grafts should allow the formation of new bone into the scaffold and the surrounding tissue and also, may have suitable physical, biological and mechanical properties which includes the pore's size and structural pore interconnectivity, chemical composition, the degradation and mechanical strength [6]. The synthetic grafts also have as advantages the osteoconductivity, free from risk of infection transfer, ensure enough supply and they are available in wide range of size and shape however, the perfect scaffold material has yet to be encountered [7].

Metal materials such as stainless steel, cobalt chromium alloy, titanium or titanium alloy were used in first place as load-bearing prostheses or fracture fixation devices which are permanent implants. Even though they show good tensile strength and relative inertness, metals have different Young's moduli which leads to stress shielding and potential fracture [8]. Calcium phosphate and Calcium silicate ceramics have been extremely employed in bone grafts since they show bio-

compatibility, low risk of adverse reactions, and generally superior tissue responses compared to polymers and metals [9].

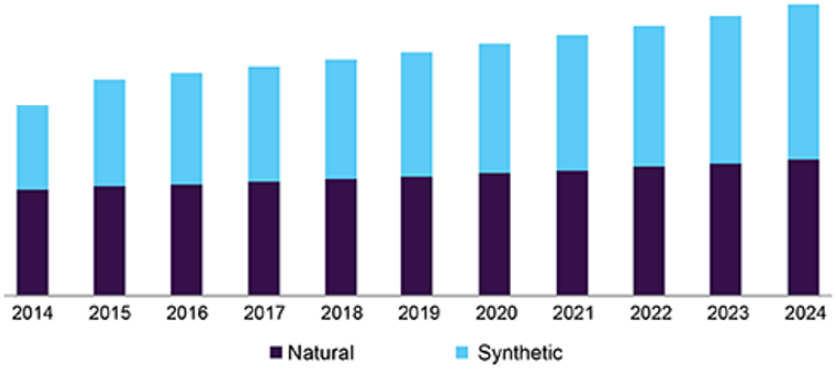

Figure 1.1: US bone grafts and substitutes market size by material. Adapted from [5].

Porous bioceramics can be produced by several methods like partial sintering, sacrificial fugitives, replica templates and direct foaming. However, they can leave residuals in the matrix, form irregular shaped pores with deficient pore's interconnectivity, it is impossible to control the porosity and the pore's size [10]. Additive manufacturing is a promising area expected to reach USD 3 billion in 2020 and to grow every year by 12.5% [11], as can be seen in Figure 1.2. This technique is quite advantageous to fabricate ceramic scaffolds since it has capacity to produce complex structures with controlled internal architecture [12]. Physicians would be able to scan the patient's body and 3D print a personalized graft using a synthetic material.

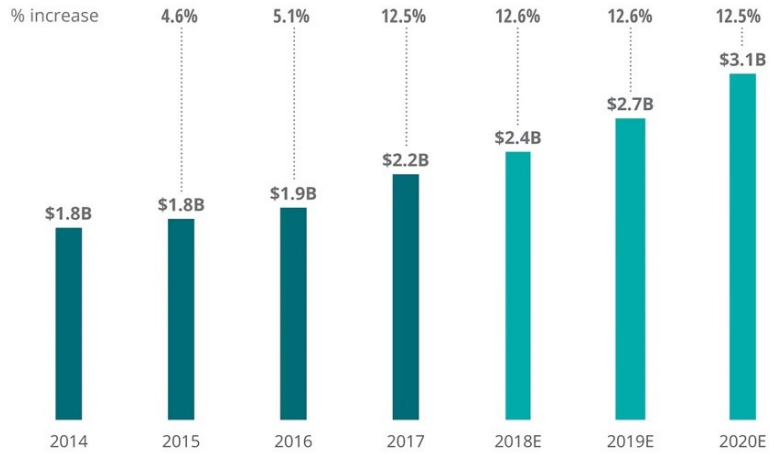

Figure 1.2: Growth of the 3D printing market until 2020. Adapted from [11].

1.1 Motivation and objective

With the increase in the average life expectancy, several health problems begin to appear, some of which affect the bone tissue. Actually, in United States of America 1.5 million individuals suffer fractures due to bone disease [13].

Existing bone grafts present many disadvantages for both the patient and the team of surgeons so that, a solution that is customizable, biocompatible and that allows through a software for example, a previous study of the surgery to be performed, would be an asset.

With the evolution of additive manufacturing technologies, the list of printable materials has expanded, making it possible to print bioceramics [11]. This brings solutions to the existing bone grafts problems, which will provide a better life-quality for the patients.

The main objective of this dissertation is to obtain a biocompatible and customizable porous ceramic bone graft with high solid content. For that, it was necessary to optimize the suspension viscosity by studying various hydroxyapatite powders, the amount of powders to be added to the suspension and the various concentrations of surfactant.

Chapter 2

Literature Review

2.1 Anatomy and Physiology of Bone

Bone is a living tissue that serves two main functions, structural support and calcium metabolism [14]. Besides that, it protects vital organs from damage, act as a reservoir for calcium and phosphate in the preservation of normal mineral homeostasis [15], is an essential part of hematopoiesis and has a role as an endocrine organ. Macroscopically, bones of the upper extremity can be divided into two different types of bone tissue, cortical bone and trabecular bone. These two tissue types have the same matrix composition however, they differ substantially in terms of their structure and function, and relative distribution both between and within bones [16]. These types of tissue can be observed in Figure 2.1.

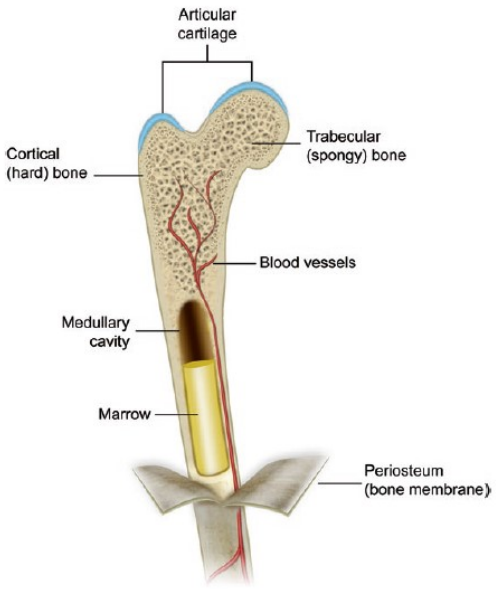

Figure 2.1: Different types of tissue that exist in the bone. Adapted from [17].

2.2 Bone functions

Bone has a vast gamut of functions divided in different categories, mechanical, synthesizing and metabolic. The mechanical category comprises the support, movement, and protection functions, the synthesizing category includes the blood formation, and the electrolyte balance, acid-base balance and detoxification belong to the metabolic category [18, 19].

1. **Body Support**: Rigid and strong bone is well suited for bearing weight and is the major supporting tissue of the body. Bones of the legs, pelvis, and vertebral column hold up the body, the jaw bones support the teeth and nearly all bones provide support for muscles.

2. **Movement**: Skeletal muscles attach to bones by tendons. Without this attachment, skeletal muscles do not have the ability to move the body. The contraction of skeletal muscles allows the movement of bones producing body movements.

3. **Protection**: Bone is hard allowing to enclose and protect such delicate organs and tissues as the brain, spinal cords, lungs, heart, pelvic viscera and bone marrow.

4. **Blood formation**: Many bones contain cavities filled with red bone marrow, which is the body's major producer of blood cells, including most cells of the immune system.

5. **Electrolyte balance**: The skeleton is the body's main reservoir of calcium and phosphate. If blood levels of these minerals decrease, they are released into the blood.

6. **Acid-Base balance**: Bone absorb or release alkaline salts to act against pH changes in the blood.

7. **Detoxification**: Bone cells remove heavy metals and other elements from the blood reducing their toxic effects.

2.3 Bone constituents

2.3.1 Bone cells

The existing bone cells were dubbed osteoblasts, osteocytes and osteoclasts, due to their different functions and sources. The osteoblasts have their origin in mesenchymal stem cells and are bone-forming cells capable of synthesize the organic matter of the matrix and to add minerals to the bone during both initial bone formation and later bone remodeling [19]. The osteoblasts produce collagen, proteoglycans and release Ca^{2+} and $PO_4{}^{3-}$ via exocytosis. As a result of these minerals concentration increase, a critical level is achieved, occurring the apatite synthesis. Bone mineralization is performed by alkaline phosphatase which is also produced by osteoblasts [20]. They can differentiate in osteocytes if the cell is trapped within the matrix, in inactive bone-lining cells if the osteoblasts remain on the surface of the new bone or can undergo in apoptosis and disintegrate. The osteocytes, classified as mature cells, are found in the lacunae and each lacunae only

has one osteocyte [21]. They interact through direct communication (gap junctional intercellular communication) and indirect communication (paracrine signaling) [22]. Osteoclasts are a type of bone cell originating from macrophage fusion that can remove bone matrix. It has a critical function in bone maintenance, repair and remodeling. For this, these cells release hydrochloric acid, collagenase and cathepsin K.

2.3.2 Matrix

Bone matrix is the part of the bone tissue where it is possible to find gaps that harbor the osteocytes and is a dynamic network composed of a broad variety of organic and inorganic constituents [23]. The organic portion of the matrix consists predominantly of type I collagen, a variety of non-collagenous proteins and minoritarily by cells [24]. The minerals are found predominantly in the form of calcium phosphate crystals with an apatite structure. The crystals of the bone matrix show imperfections and are not exactly the same as hydroxyapatite ($Ca_{10}(PO_4)_6(OH)_2$). These minerals form deposits of dense particles along the osteocollagenous fibers. The inorganic portion of the matrix occupies 65% of the matrix and the organic portion 35% of the matrix. The precise composition of the matrix may be subject to change over time due to nutrition and biomineralization, and it can also be found traces of minerals such as magnesium, sodium, potassium and carbonate [25]. The minerals resist compression (crumbling or sagging when weight is applied) so, when bones are deficient in calcium salts, they become soft and bend easily. The collagen fibers of bone give it the ability to resist tension, so the bone can bend slightly without snapping. Without collagen, the bones become very brittle [18].

2.4 Cortical/Compact Bone vs. Trabecular/Spongy Bone

Cortical bone is also called compact bone, it forms the hard outer layer of bones and it has higher density than trabecular bone. Microscopically, this type of bone consists in concentric lamellae, osteons, Volkmann canals, blood vessels, nerves, canaliculi and osteocytes [18]. The basic structural unit of compact bone is an osteon, which is constituted by a central canal and its lamellae which in turn is constituted by layers of matrix concentrically arranged around a central canal. To connect the central canals, transverse or diagonal passages called Volkmann canals are found, containing blood vessels and nerves. The lacunae is a elongated space that is occupied during the life-time by a bone-cell or a bone-corpuscle [18, 26, 19]. The osteocytes near to the central canal receive nutrients from the blood vessels and pass them along through their gap junctions to the neighbouring osteocytes, receiving waste from them and convey them to the bloodstream. Trabecular bone, also known as spongy bone, is a heterogeneous and anisotropic material and present less bone matrix and more space than compact bone becoming, in this way, highly porous [19]. This tissue can be found in the epiphyses and metaphyses of long bones and in the vertebral bodies [27]. A single trabeculae comprise groups of parallel lamellae limited by cement lines, which are oriented parallel to trabecular surfaces. Comparing trabecular bone with cortical bone it was found that the first has higher surface to volume ratio and a considerable bone remodelling

than compact bone [27]. These tissues have different mechanical properties [28]. The Young's Modulus, the compressive strength and the flexural strength of cortical bone are bigger than that of the trabecular bone due to the dense structure and with higher concentration of apatite minerals of the compact bone [29]. These values can be observed in Table 2.1.

Table 2.1: Cortical and trabecular bone properties. Adapted from [29].

Property	Cortical Bone	Trabecular Bone
Young's Modulus	7-30 GPa	0.05-0.5 GPa
Compressive strength	100-230 MPa	2-12 MPa
Flexural strength	50-150 MPa	10-20 MPa

2.5 Bone properties

Bone is an adaptive tissue, and very sensitive to immobilization or dynamic activity and to high load levels. When bone is subjected to load, the internal framework of the trabeculae undergoes adaptive changes, occurring then changes in the external cortical portion of the bone making the bone stronger in order to resist to that sort of loading. These changes occur due to the anisotropic characteristics of the bone tissue, indicating that the behavior of the bone will change depending on the direction of the load application. Since bone is accustomed to receive loads in the longitudinal direction, it becomes stronger in that direction. Bone is a viscoelastic tissue, i.e. the tissue responds in a different way depending on the speed to which the load is applied and the load application time. When the load is applied, the bone is deformed and after the load is removed the bone goes back to the original format due to his elastic response. Bone is a highly viscoelastic material because of the large amount of collagen content. The stress-distension curve allows to determine if a material is hard, flexible, fragile, strong or weak [30]. Bone provides a plastic response which is the deformation of the tissue undergoing non-reversible changes of shape in response to the forces applied. This happens because the external fibers of the bone tissue start to collapse, occurring micro-breaks and the material detach from the bone. Strength is the ability of the bone tissue to resist the influence of the external forces acting upon it. This characteristic can be analyzed in terms of storage of energy, the area under the load-deformation or stress-distension curve. The modulus of elasticity is a material property, that report the stiffness which represents the material's ability to resist deformation [31] and is, therefore, one of the most important properties of the solid materials. The stiffness can be characterized by Young's module, described by the slope of the linear region of the strain-stress curve when tested under tension. The modulus of elasticity (i.e. the stiffness) is higher when bone has high mineralization. This makes the bone stronger, but it lowers the toughness, becoming less capable of absorbing shock and strain energy. Cortical bone and trabecular bone have different stiffness. The first can sustain bigger stress but less strain before failure, and it's stiffer than trabecular bone. The second has a greater capacity to store energy compared to compact bone because is more porous and filled with body fluids

such as blood and marrow. Over time, bone loses physical properties, such as toughness, Young's modulus, and mechanical strength as can be seen in Figure 2.2 [32].

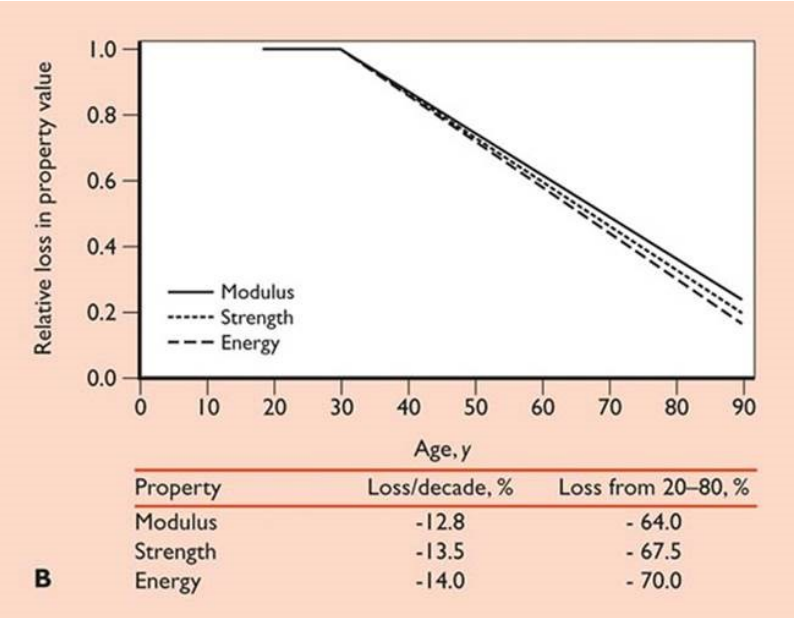

Figure 2.2: Relative Loss in property value by age. Adapted from [33].

2.6 Bone Remodelling

Bone is a living organ that undergoes remodeling throughout life. This process is essential to allow the substitution of the youthful bone with a bone which have better mechanical competence, to substitute microfractured bone and to guarantee a correct calcium homeostasis [34, 35]. For bone remodelling to occur, a brief assembly of osteoclasts, osteoblasts and capillary blood supply (basic multicellular unit) migrate to the surface of the injured bone, removing the matrix and replacing it with new bone matrix [19]. The process combine five steps: activation, resorption, reversal, formation and termination [36]. In the activation phase, osteoclast precursor cells are recruited and activated, the lining cells detach from the surface of the bone and occur the formation of multinucleated preosteoclasts through the fusion of multiple mononuclear cells. Thereafter the multinucleated preosteoclasts bind to the mineralized bone matrix forming sealed regions [37].

Ending the activation phase, begins the resorption phase that lasts approximately 2 weeks. The binding promote the formation of a ruffled membrane, creating an isolated hemivacuole between the osteoclast and the bone matrix. The osteoclasts excrete hydrocloridric acid and acidic proteins into the vacuole in order to promote the proteolytic enzymes activation, which have their activation peak at low pH. These enzymes have as function the degradation of the organic constituents of the matrix [37, 36]. Resorption ends when the osteoclasts undergo apoptosis. This is followed by the reversal phase that lasts between 4 and 5 weeks.

Reversal phase makes the transition between the resorption stage and the formation stage and is still not well understood. One of the theories assert that the resorption release growth factors from the bone matrix inducing osteoblast proliferation and differentiation. Another theory says that this transition is regulated by a strain phenomenon [36, 37].

The formation phase takes approximately 4 months to be completed. Initially, osteoblasts synthesize organic matrix, called osteoid, and release vesicles which allow the initiation of the mineral deposition through the release of calcium and phosphate, and the destruction of inhibitors of mineralization. Termination occurs when osteoblasts die by apoptosis, when they incorporate themselves into the matrix, turning into osteocytes or when they convert into bone-lining cells [36, 37]. The remodelling cycle is illustrated in Figure 2.3.

An equitable balance between resorption and formation should be achieved in order to obtain a homeostatic equilibrium. In this way, the aged bone is replaced by new tissue so that it adapts to mechanical load and strain. According to Wollf's law, if loading on a bone increases, the bone will remodel itself over time to become stronger to withstand those stresses [18].

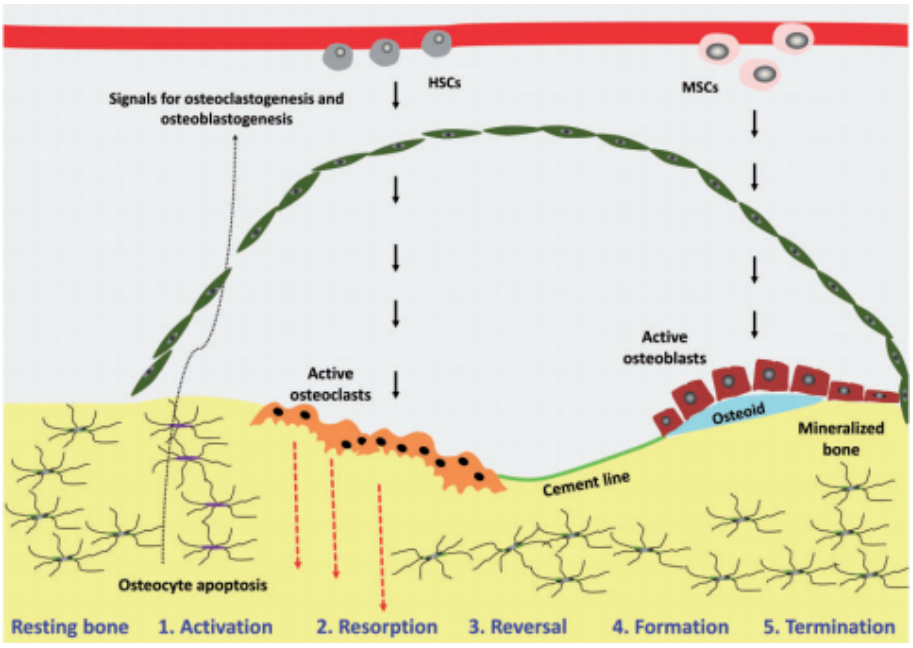

Figure 2.3: Bone remodelling cycle. Haemopoietic stem cells (HSCs) and mesenchymal stem cells (MSCs). Adapted from [36].

2.7 Diseases associated to bone

The bone loss can occur due to bone defects or to structural loss. The structural loss is caused by bone inflammation, bacterial infection and metabolic diseases. Regarding inflammation, the bone loss takes place on account of local resorbing factors that are synthesized by hematocytes. This effect also appear in the presence of bacteria, who are responsible for releasing products that can corrupt the bone. Periodontal disease and osteomyelite are examples of bacterial infections [38].

Periodontal disease is an infection of the structures around the teeth such as gums, cementum, periodontal ligament and the alveolar bone. Osteomyelite is a bone infection usually caused by bacteria [39] and is associated with the placement of prostheses, fractures, bone reconstruction surgeries and it is also found in patients with diabetes or vascular insufficiency.

Metabolic diseases occur due to abnormalities of minerals such as calcium, phosphorus, magnesium or vitamin D. This type of diseases may result in bone pain and loss of height (in consequence of vertebra compression) which may lead to fractures. Osteopenia, osteoporosis, Paget's disease of bone and rickets are some of this type of diseases. Osteopenia is a condition in which bone mineral density is below the normal and can be considered a forerunner of osteoporosis. Osteoporosis is a disease defined by deficient bone mass and microarchitectural deterioration of bone tissue, since bone resorption exceeds bone formation [40], leading to enhanced bone fragility and a consequent increase in fracture risk [41]. Paget's disease of bone is defined by a disorganized bone remodeling, and as has symptoms bone pain, bone deformities, headache, nerve root compression and fractures [42]. The origin of this disease is not yet known, but it is thought that is due to genetic factors or environmental factors namely viral infections [42]. At the first place, large and numerous osteoclasts initiate an intense bone resorption, recruiting osteoblasts that begin to produce bone matrix. However, bone resorption is happening at the same time making bone mineralization inefficient, and therefore normal lamellar bone is replaced by woven bone. Finally, bone resorption decreases remaining an disorganized bone which is weaker than the normal bone [42, 13]. Rickets and osteomalacia are bone diseases caused by lack of vitamin D, phosphate or calcium. These are crucial nutrients for the development of strong bones. Rickets disease affects children while osteomalacia affects adults, however both experience similar conditions. The mineralization of the growth plate is insufficient leading to an accumulation of osteoids in the bone tissue which causes the bone to become weak.

Hormonal disorders are another factor that perturb bone homeostasis. Hyperthyroidism results of an exaggerated production of thyroxine hormone by thyroid gland. This hormone stimulates bone resorption, reducing the density of bone, which can lead to osteoporosis and in an increase of the fracture rate [43]. Also, the lack of gonadal hormones, such as testosterone and estrogen, in children and young adults may contribute to severe osteoporosis. Additionally, higher production of cortisol will cause Cushing's syndrome, which is also harmful to bone health[13].

Some types of medicines cause bone loss, if used for long periods of time. An example is medicines with glucocorticoids, which, when taken in excess will stop bone growth in children [13].

Bone cancer affect the bone mineral density, not only due to the effect of cancer cells but also due to the therapies used in the cancer treatment. The cancer destroy bone tissue in order to settle itself and grow, and eventually form metastases [44].

Fractures, trauma, inappropriate fracture fixation will also increase the probability of bone density loss [45].

2.8 Bone grafts

As previously mencioned, bone is a tissue that is subjected to renewal and repair processes during bone remodelling, which can be seen during normal fracture healing. However, there are clinical conditions where the remodeling process is not enough to establish the normal bone structure, like trauma, infections, tumor removal surgery and skeletal anomalies, or cases in which the regenerative process is compromised, including avascular necrosis, atrophic nonunions and osteoporosis [46].

In order to solve this problem, the physicians needed to remove bone from another part of the body and shape it to fit the area where it is needed. However, this bone graft can lead to swelling, nerve injury, bone graft rejection, inflammation and may not fit perfectly into the defect [3]. Bone grafts can be defined as materials of natural or synthetic origin used as a filler or scaffold to facilitate bone formation and promote wound healing [47].

Bone grafting is conceivable since bone tissue can regenerate entirely if provided the area into which it has to grow. As natural bone grows, it generally substitute the graft material completely, resulting in a fully functional new bone. There are different types of grafts, autografts, allografts, synthetic variants and xenografts [47]:

1. **Autografts**: Tissue transplanted from one region of the body to another in the same individual.

2. **Allografts**: The allografts are grafts harvested from an different individual, but of the same specie, of the one who receives the graft. Allograft bone is taken from cadavers that have donated their bone so that it can be used for living people who need it.

3. **Synthetic variants**: Composite of flexible hydrogel-hydroxyapatite (HA) with mineral organic matrix ratio similar to human bone. This artificial bone can be composed of calcium phosphates, bioglass and calcium sulphate, and can be combined with growth factors, ions or mixed with bone marrow aspirate to increase biological activity.

4. **Xenograft**: A graft of tissue taken from a donor of a species and grafted into the body of another species.

2.9 Bone graft properties

One of the multiple purposes of a bone graft is to provide a healing facilitator structure that fills the bone defect and that enables the settlement of osteoinductive molecules and/or osteogenic cells [48]. For that, the material used to fabricate the graft should have several qualities such as biocompatibility, osteocondutivity, porosity and adequate mechanical properties.

2.9.1 Biocompatibility

Biocompatibility is defined as a *"property of being biologically compatible by not producing a toxic, injurious, or immunologic response in a living tissue"* [49]. The graft constituting materials, such as monomers, initiators, cross-linking agents, emulsifiers, stabilizers and degradation products, have biocompatibility as a prerequisite. Calcium phosphate (CaP) ceramics, such as hydroxyapatite (HA) and tricalcium phosphate (TCP) have chemically similarities with the inorganic component of natural bone tissue, revealing great biocompatibility.

2.9.2 Osteocondutivity

Bone grafts need to have a vital characteristic called osteoconductivity, which allows the growth of bone in its surface, channels, pipes and also into pores [50]. This permits the adhesion of cells, their proliferation, migration and bone precipitation. As said before, CaP ceramics are similar to the inorganic phase of bone revealing also a great osteoconductivity. To improve osteocondutivity, it is increased the scaffold microporosity since a higher surface is obtained [17].

Some biodegradable polymers exhibit osteocondutivity as well. The attachment of these polymers with specific peptides derived from ECM proteins may increase the osteocondutivity, promoting growth and migration of osteoprogenitor cells as well as osteoblasts. Another approach is to fabricate scaffolds with collagen fibrils which mimic the nanostructure of ECM in natural bone tissue.

2.9.3 Porosity

Porosity is defined as the percentage of void space in a solid and it is a morphological property independent of the material. Pores are necessary for bone tissue formation because they allow blood vessels and surrounding bone to grow into the bone graft and promote migration and proliferation of osteoblasts and mesenchymal cells. In addition, a porous surface improves mechanical interlocking between the implanted biomaterial and the surrounding natural bone, providing better mechanical stability at this critical interface. Various methods may be used to create porous scaffolds depending on material properties and desired pore architecture [51]. The bone scaffolds should have interconnected pores with at least 100 μm in diameter for the diffusion of oxygen and essential nutrients for the survival of the cell. However, macropores with a diameter of 200-350 μm are also important since it was found that they are optimum for bone cellular in-growth [52]. Although increased bone graft porosity may increase permeability, the modulus will be sacrificed [53].

2.9.4 Mechanical Properties

The cooperation between HA crystals and elastic collagen fibers in the nanoscale structure of bone contribute to its unique mechanical properties, making bone difficult to substitute using synthetic

materials [54]. Metals, such as titanium and stainless steel, are usually used in orthopedics, because of the higher strength compared to bone [55]. However, these implants absorb most of the stimulating forces, which cause a phenomenon called stress shielding effect. This phenomenon consists in the bone resorption around the implant. Also, metals show elastic modules with different values from those of natural tissue having therefore a mismatch of various mechanical properties. The ideal scaffold should be designed to match the mechanical properties of the specific bone it will replace [48] and should have enough balance between mechanical properties and porous architecture to allow cell infiltration and vascularization, which is the key to the success of any scaffold.

2.10 Bioceramics

Ceramic materials are inorganic materials consisting of chemically bonded metallic and nonmetallic elements. They may be crystalline, non-crystalline or a mixture of both. Most of them have high mechanical strength at high temperatures but tend to be brittle and typically have a high compressive strength and low ductility, providing high resistance to deformation [56]. The matrices that have been used to bone regeneration are calcium phosphates, calcium sulphates and bioactive glasses. There are four types of bioceramics, type 1 (nearly inert), type 2 (porous ingrowth), type 3 (bioactive) and type 4 (resorbable). Figure 2.4 shows the bioactivity spectrum for various bioceramic implants already on the market.

1. **Nearly Inert**: The reaction with the tissue is very small, happening on a small scale, after a long time and are used when no significant reaction is expected. Alumina (Al_20_3) is an example of type 1 showing a hexagonal compact structure and greater thermodynamic stability. The bond strength is so great between Al and O that they do not react with the environment. They are used in joint prostheses, but also in engine sails, where they resist high temperatures without degrading. $Al_2O_3 - Si_3N_4$ is an example of a nearly inert bioceramic implant already on the market.

2. **Porous ingrowth**: Allow the growth of cells into their pores occuring a stabilization of the prosthesis by mechanical (interlocking) and biological action i.e, the formation of bone bridges occurs. It is a classification that does not depend on composition. Increasing the interfacial area between the implant and tissues results in increased resistance to implant movement. The limitation is that the pores must be relatively large (more than 50-150 μm) because it is necessary to have vascularization in the new connective tissue. Porous bioglass and porous hydroxyapatite are examples of this type of bioceramic.

3. **Bioactive**: Intermediate between inert and resorbable. Preserved in the body for longer, stimulating bond between the tissue and the material. So, it is important that the composition of the ceramic and bone are the same. A biological response occurs at the interface between the tissue and the material. Bioglass, ceramic glasses and bioactive ceramics are examples of this type of bioceramic.

4. **Resorbable**: React with the body, degrading. One example is calcium sulphate (gypsum-used as bone cement) and other bone cements. They have the advantage of not having to remove the material later since it is reabsorbed. The disadvantages are that they may disappear too quickly so that the mechanical properties fall immediately after their placement, and sometimes it may be difficult to match the rate of resorption to tissue replacement. The alpha-phosphate, macroporous and thin-walled, is at the limit of being resorbable ($Ca_3(PO_4)_2$). This has a calcium/phosphorus ratio of 3:2, hence they are more resorbable than HA, which has a calcium/phosphorus ratio of 10:6.

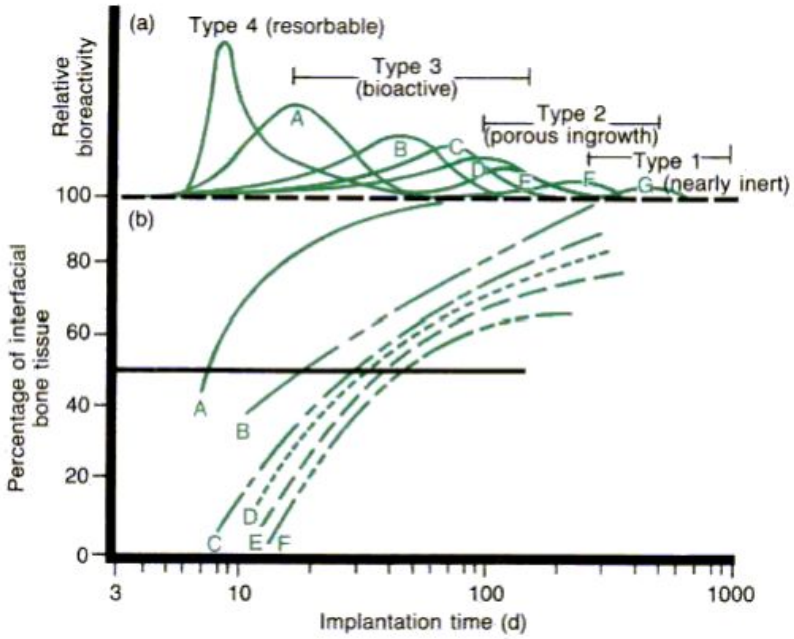

Figure 2.4: Bioactivity spectrum for different bioceramic implants. (a) relative rate of bioreactivity, (b) time dependence of formation of bone bonding at an implant interface. (A) 45S5 Bioglass ®, (B) KGS Ceravital ®, (C) 55S4.3 Bioglass ®, (D) A/W glass ceramic, (E) HA, (F) KGX Ceravital ® and (G) $Al_2O_3 - Si_3N_4$. Extracted from [57].

2.10.1 Calcium Phosphates

Calcium phosphates are composed by calcium and orthophosphate ions which are also present in the mineral components of bone, and are highly biocompatible [58] being therefore suitable for synthetic bone graft production [59, 60]. The bioactivity of calcium phosphates may vary with the calcium phosphate ratio, the cristallinity and with the phase purity.

The choice of the calcium phosphate material should be based on their properties combined with the final purpose. One important property is the resorption rate which is affected not only by the geometric properties but also for the chemical composition of the calcium phosphate [60]. Geometric characteristics are related with the interconnectivity of the pores and with the porosity.

Hydroxyapatite (HA) and β-tricalcium phosphate (β-TCP) have an augmented capacity to bond with bone tissue and show a biocompatible nature, which makes them the most popular among calcium phosphates [59].

Hydroxyapatite (HA)

Hydroxyapatite is a biocompatible calcium phosphate with a chemical structure similar to the inorganic component of the bone [61]. This bioceramic can be found in the market either from natural sources or as a synthetic material. Synthetic hydroxyapatite is a stoichiometric apatite with a chemical formula of $Ca_{10}(PO_4)_6(OH)_2$ and a calcium phosphate ratio of 10:6. Natural hydroxyapatite is a non stoichiometric apatite, that show traces of $C0_3$, Mg, Na, F and Cl and with a calcium phosphate ratio lower than 1.67 [62]. Hydroxyapatite has low solubility and high stability inside the human body. It was found that the closer to 1.67 is the calcium phosphate ratio, the greater the stability, however if this value decreases the bioactivity is improved [62].

Due to the properties mentioned above this calcium phosphate brought great interest to the biomedical materials field. The clinical applications of hydroxyapatite continue to emerge, but nowadays it is used as a bone filler, as a bone tissue engineering scaffold, as a bioactive coating, as a delivery system and as a drug/proteins/genes loading [63].

Tricalcium phosphate (TCP)

Tricalcium phosphate has a nominal composition of $Ca_3(PO_4)_2$ with a calcium phosphate ratio of 1.5. Two different crystallographic configurations can be found, α-TCP and β-TCP which is more stable than the first.

TCP is a biocompatible and bioresorbable material which shows no osteoinductive activity [64].

This ceramic has higher biodegradation rate than hydroxyapatite so that, in order to adapt the material's biodegradation rate, biphasic calcium phosphate materials with different levels of HA and TCP are prepared [59].

The dental medicine field is the one that most benefits from these materials since they allow filling in periodontal defects in bone and repair cleft palates. Also, it can be used as a scaffold for orofacial fractures, as a coating in metallic materials and as drug carriers [65, 66].

2.10.2 Porous ceramics

2.10.2.1 Processing methods of macroporous ceramics

Porous materials can be classified in three classes, according to pore diameter. Materials with a pore diameter bigger than 50 nm are designated by macroporous, between 2 nm and 50 nm are nominated mesoporous and materials with a diameter smaller than 2 nm are called microporous [67]. Trabecular bone is a macroporous tissue, as seen in subsection 2.9.3, thus a macroporous graft is required. In this context, the research work was focused in the processing methods of

macroporous ceramics. Figure 2.5 ilustrates the different processing methods: partial sintering, sacrificial fugitives, replica templates and direct foaming.

1. **Partial sintering**: Partial sintering is one of the most frequent approaches to obtain porous ceramics, and involves the partial sintering of ceramic aggregate particles [67, 68]. It consists in lowering the processing temperature or pressure during the consolidation which will increase the porosity, interconnectivity and pore size [67, 69]. Also, the porosity can be increased with the addition of pore forming agent [68]. The porosity obtained with this process is, generally, inferior to 50%.

2. **Sacrificial fugitives**: In this process, pore forming agents like some organics or carbon powders are added to the ceramic slurry. During sintering the agents burn out, leaving behind a porous material [68]. The agents should be homogeneously mixed with the ceramic slurry to obtain an uniform and regular distribution of pores. The pore size and shape are dependent of the pore forming agents morphology and the porosity increases with the quantity increase of these agents. The porosity obtained with this process alternate between 70% and 80 % [67].

3. **Replica templates**: Replica templates is a very popular method. A sponge or a cellular natural structure is soaked into a ceramic slurry until all the pores are filled with the suspension. Then, the suspension excess is removed through rollers. The sintering stage allows to remove the sponge or the cellular natural structure and the densification of the ceramic. The resulting structure has the same morphology of the original model. The obtained porosity varies between 40% and 95%, however some interconnectivity is lost and the pieces show low mechanical properties [70].

4. **Direct foaming**: Direct foaming consist in the addition of gas or air to the ceramic slurry which is stabilized using, generally, a surfactant followed by drying and sintering. The consolidated structure shows porosities below 90 %, and the method is cheap and environmentally-friendly [67].

Despite the fact that the processes cited above showed high values of porosity and interconnectivity, they can not control the material's microstructure [70] since the connectivity is an arbitrary result affected by the processing parameters.

Recently, a new processing method capable of creating structures from computed-aided designs (CAD), has gained popularity. This method unlike the previous ones allows to control the material's microstructure. It is called additive manufacturing and encompasses several techniques [71].

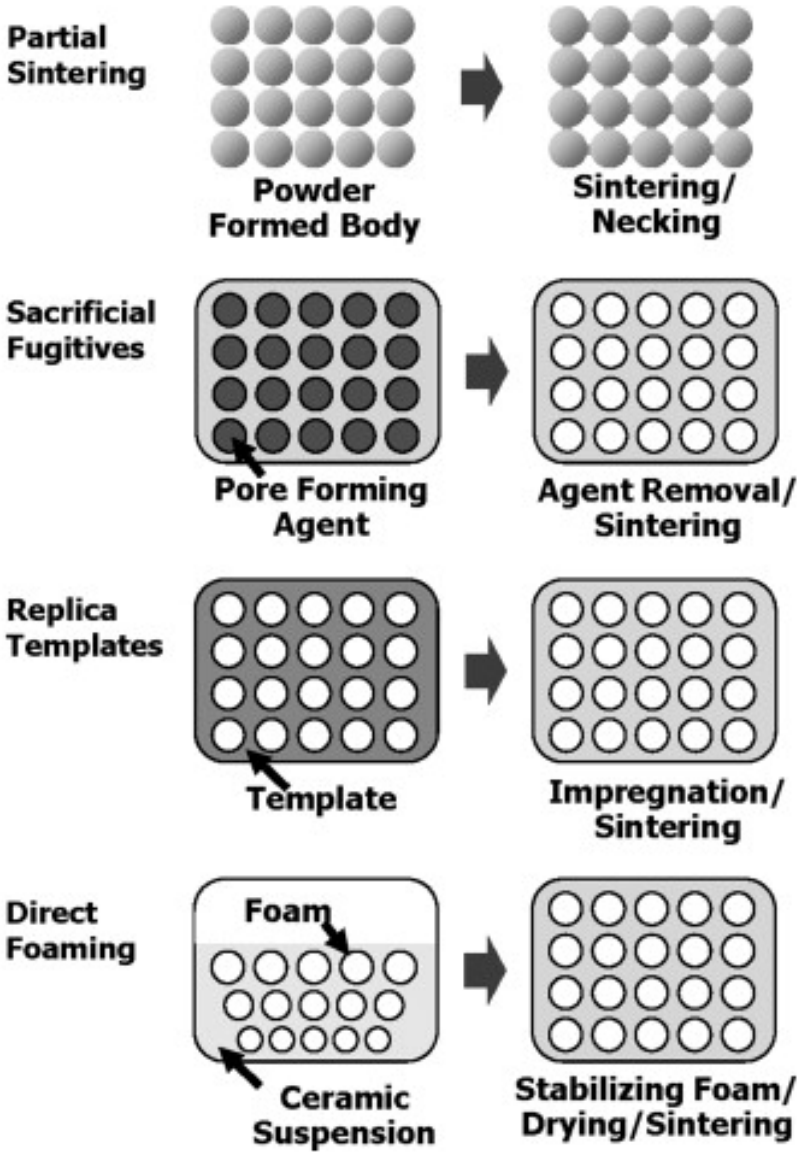

Figure 2.5: Different processing methods of macroporous ceramics. Adapted from [67].

2.11 Additive Manufacturing

2.11.1 Biomodel

Although autografts, allografts and xenografts are the most commonly used grafts nowadays, they present several complications. The concerns regarding autografts are due to limited supply and to donor site complications and both allografts and xenografts can contribute to the transmission of diseases and other infective agents. One of the problems common to the types of grafts mentioned above is that they do not fit perfectly into the defect [72]. To address these limitations, customized synthetic bone substitutes began to appear. This required an compromise between computer-aided design (CAD) and additive manufacturing techniques [73]. Through a computed tomography scan

(CT scan) or a magnetic resonance imaging a biomodel is created.

Lohfeld et al. defined a biomodel as an entity that replicates the geometry or morphology of a biological structure, which can be realized in either a computer-based form or a solid physical form [74]. Macro scale virtual models reproduce the precise structure of the tissues, which is extremely useful in the surgerie's planning reducing the risk to the patient. Biomodels can be manipulated by CAD software, which is usually used in designing implants and prostheses, which can estimate the risk of fracture and improve some features such as microstructure, shape and size [74].

2.11.2 STL file

The STL file was designed in 1987 and is a file format native to the stereolithography CAD software created by 3D Systems Inc. STL is an abbreviation to "Standard Triangle Language" or to "Standard Tessellation Language" and it is broadly used for rapid prototyping, 3D printing and computer-aided manufacturing [75, 76]. The STL file creation process remodel the continuous geometry in the CAD file into small triangles, or coordinates triplet list of x, y and z coordinates and the normal vector to the triangles. Depending on the complexity of the surface, the number of triangles varies. If the surface complexity is greater, the number of triangles will also be larger, if the surface complexity is smaller, the number of triangles will be smaller. The STL file only describes the surface geometry of a three-dimensional object without any representation of color, texture or other usual CAD model features. There are other types of files such as stereolithography contour (SLC) and SLI from 3D Systems, CLI from EOS, Hewlett-Packard graphics language (HPGL) from Hewlett-Packard, stereolithography contour from Stratasys, and F&S from Fockele and Schwarze and initial graphics exchange specifications (IGES) [77].

2.11.3 Additive Manufacturing of Ceramics

Additive Manufacturing (AM) processes are versatile, flexible and high customizable [78] and are also known as rapid prototyping and solid freeform fabrication [79]. AM describes a class of technologies in which is created a physical structure (3D) by layering materials one by one based on a digital model [80]. These processes have been gaining interest in industries and also at academic level because of their ability to create complex geometries with customizable material properties [81]. Ceramic materials generally have low ductility, high crack damage sensitivity, low toughness that combined with high hardness and high melting temperatures make them difficult to work with during the manufacturing [82]. However, AM processes have the capability to control the architecture which is beneficial because scaffolds can be designed and fabricated to fit the patient's needs [83]. Below it is presented the processes of additive manufacturing for ceramics, such as vat polymerization, material extrusion, direct energy deposition, powder bed fusion, binder jetting and sheet lamination [84]. Figure 2.6 shows the seven processes of additive manufacturing.

1. **Vat polymerisation**: Vat polymerisation uses a vat where an photopolymer resin is placed. An UV laser is applied in order to draw a pre-programmed design or shape onto the surface

of the photopolymer vat, which is sensitive to UV light and in this way, the resin solidifies and forms a single layer of the desired 3D object. After each layer polymerization, the build platform goes up in order to allow the resin to spread and descends for a height equivalent to the height of the previous one plus the layer thickness, and then the polymerization occurs [85, 86]. This process is repeated until the 3D structure is completed. The advantages of the process is the high-resolution capacity, the high-layer speed capacity, low-imaging specific energy, can build simple or complex structures with very good accuracy and surface finish and can build parts with specific characteristics. The disadvantages are that is a complex process, require support, the materials used are expensive, is limited in materials that can be used, it is only applicable for photopolymers which are not stable over time and have not well defined mechanical properties, and the build process is slow [86, 87, 88]. Stereolithography and Digital Light Processing are examples of this process.

2. **Material Extrusion**: In this process, the material is deposited through a nozzle being possible to regulate the extrusion force and plunger velocity [89]. The material is heated and the nozzle moves horizontally depositing it into the required cross section area of the desired object. Finishing the layer, the platform moves vertically, positioning itself in order to deposit the next layer. The process is repeated layer-by-layer until the object is completed. The material for material extrusion must have a high solid loading in order to avoid shrinkage and cracking due to sintering, have a homogeneous particle distribution to ensure a constant flow and to avoid flaws due to agglomerates, minimize the entrapped air, solvent migration and their sedimentation should be avoided to ensure constant flow and storage stability. In addition, the particle size, distribution, rheology, interface properties and solidification kinetics of the feedstocks should be suitable for the desired structure and the binder phase should be easy to drain, dry or burn out [86]. The advantages of this technique are that it can handle higher-viscosity feedstock materials and higher extrusion temperatures [90], the fabrication system is simple and low cost, the final structure have high density, it is capable to produce parts with multiple material and has a small waste of material [91].

3. **Direct Energy Deposition**: The operation method of direct energy deposition is similar to the material extrusion process. However, the nozzle can move in multiple directions and the material, provided in wire or powder form, is melted using a laser, electron beam or plasma arc upon deposition [92]. DED is used frequently to material repair since new material can be deposited in the damaged part, and it has ability to control the grain structure and the produced pieces reveal good surface quality [93]. On the other hand it may require post processing and is limited in material [94].

4. **Powder Bed Fusion**: It consists in a laser that heats the powder to just below or right at the melting point of the material, fusing the particles together creating a compact object. The platform lowers at a distance equal to the thickness of the layer produced and a recoater applies a new layer of powder on top. This process is repeated until the 3D model is totally printed. When the structure cools down, the structure and the powder excess are removed

[86, 95, 96]. Powder bed fusion can be used with a variety of materials, there is no need for support structures because the powder bed is used as the support, has good mechanical properties, low material cost and have good accuracy. However, the feature resolution depends on laser-beam diameter, materials may degrade during the process because of the temperature, the structure may have undesired porosity, it is hard to remove the trapped powder and is a complex and expensive equipment [95, 87].

5. **Binder Jetting**: The powder bed fusion consists of an ink-jet head that moves applying droplets of the binder solution to the powder bed, gluing the powder together. When a certain layer is finished, the build piston is lowered a distance equal to the thickness of the layer produced and the powder delivery piston raises the powder that is spread on top of the finished layer through the roller. This process is repeated until all the structure is formed and the excess of powder is removed [86, 95, 96]. The advantages of powder bed fusion are the high variability of material choices, good mechanical properties, low cost, is a quick process, low waste of material, low imaging specific energy, it is possible to print an object with multiple colors and they have multi-material capabilities through multiprint-heads [97]. However, the resulting object can suffer from a rough surface quality, some materials need to be post-processed, the process works well only with a values of viscosity between 10 and 12 mPa·s [98], sometimes it is hard to remove trapped materials, have low to medium resolution, the powder particles may not bind well, and it is always necessary to bind powders [95].

6. **Sheet Lamination**: The object is built through an additive process that can make different structures with different shapes and sizes by shacking, bonding and cutting the sheet layers of a material [99]. This process is performed by joining a sheet to a substrate with a heated roller, based on the 3D model a carbon dioxide laser traces the desired dimensions of the structure cutting the outline of each layer and crosshatches the waste material within and around the layer for easy removal after the structure is completed [96]. The layers are bonded to each other through pressure using a hot roller, the sheet is moved away, a fresh sheet of material is rolled into position and the platform is lowered one layer deep, to receive the next layer. This process is repeated until all the structure is completed. The resulting structures present very low internal tensions which prevent distortion, shrinking and deformation, have high durability, low brittleness, low fragility, it is possible to produce large parts with good finishes, machine and process costs are lower than with other RP systems and there is no need to post-processing or supporting structures. The disadvantages are the low accuracy, low detail reproduction, low durability of small part features, a significant waste of material, internal cavities are difficult to be built and the material is dependent from the direction of the machinability [88, 100].

7. **Material Jetting**: In this process a movable printhead deposits droplets of a photosensitive liquid which solidify when exposed to ultraviolet light. Material jetting has low waste,

produce samples with a smooth surface finish and high dimensional accuracy, however, it requires support material and the materials are limited [101].

All of the processes have as an input an STL file containing the design of the structure to be printed. In particular, hydroxyapatite can be printed by all of the additive manufacturing processes, although each of them has their advantages and disadvantages. Material extrusion techniques are the most widely employed 3D printing strategies for tissue engineering, which have led to remarkable progress in the field [102, 91].

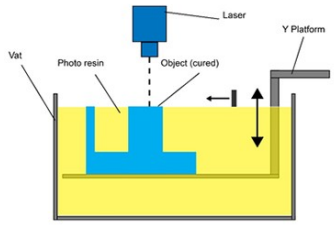

(a) Vat polymerisation process.

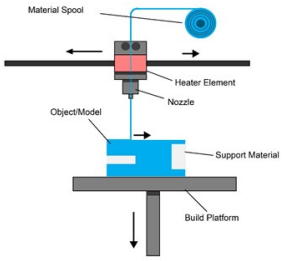

(b) Material extrusion process.

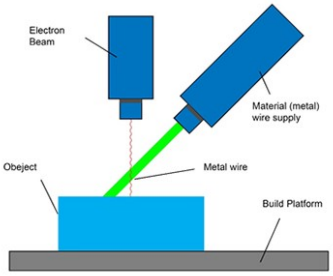

(c) Direct energy deposition process.

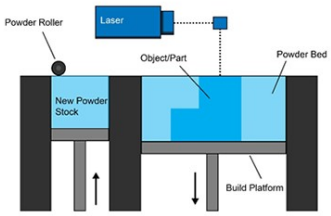

(d) Powder bed fusion process.

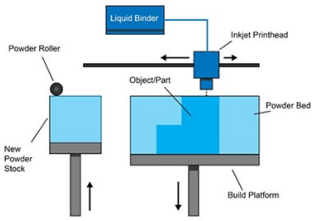

(e) Binder jetting process.

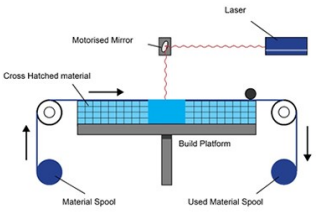

(f) Sheet Lamination process.

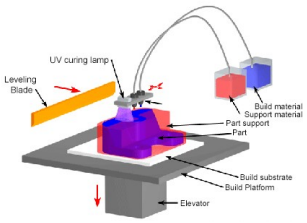

(g) Material jetting process.

Figure 2.6: Seven processes of Additive Manufacturing. Adapted from [103, 104, 105, 106, 107, 108, 109].

Chapter 3

Materials and Methods

3.1 Raw materials

3.1.1 Resin

The resin is a printing vehicle that needs to be removed to obtain the purest ceramic possible after processing. It must be organic so that, when it heated up in the kiln it burns-out completely, leaving no residue behind. In this way it is obtained an inorganic structure that corresponds to the ceramic. Furthermore, the resin should allow the incorporation of solid-powders maintaining the needed characteristics for the DLP printer. With this in mind, an exhaustive search was carried out for the existing resins in the market taking into account the price and characteristics such as viscosity and density. Table 3.1 shows some of the resins found in the market which comply with the conditions above described. The chosen resin was the Resin 1 not only for the price, but also because it has already been used in previous works by the research group that is engaged in this project, with pretty good results. Resin 1 is a photopolymer curable resin base suitable for DLP and SLA 3D printing and is designed for experimental use, which allows, together with solid powders, to create a 3D printable resin.

The firing schedule and maximum sintering temperature for Resin 1 is dependent of the sintering temperature of the ceramic material. A thermal cycle is proposed by the company, in order to prevent the appearance of cracks on the produced 3D piece.

Table 3.1: Examples of resins in the market and their associated properties and price.

Resin	Viscosity @ 25ºC	Density	Price (per L)
Resin 1	-	-	249.95 €
Resin 2	552 mPa·s	1.10 g/cm^3	258.00 $
Resin 3	250-325 mPa· s	1.02-1.12 g/cm^3	249.00 €

3.1.2 Hydroxyapatite powders

Four different hydroxyapatite synthetic powders were used which were acquired in four different companies and named as HA1, HA2, HA3 and HA4. All these powders obey to ISO 13779-6 for surgery implants.

3.1.3 Dispersant

The hydroxyapatite powders may form aggregates, which will cause a decrease in strength and reliability of the final printed piece [110]. In order to improve particle separation and to prevent aggregation or deposition of the hydroxyapatite particles during 3D printing, sodium lauryl sulfate was used as a dispersant.

3.1.4 Non-polymerized resin cleaning liquid

After the pieces are printed it is necessary to remove residues of unpolymerized resin that may have remained. This is an crucial step, since these residues may develop cracks, delamination and/or swelling [111]. For this purpose, three different solvents (S1, S2 and S3) were evaluated as cleaning liquids.

3.2 Slurry preparation

In order to obtain a ceramic piece, a slurry was prepared which was constituted by a photopolymer resin, a hydroxyapatite powder and a dispersant. The synthetic hydroxyapatite powders were maintained overnight in a oven (J.P.Selecta, s.a., Spain) at 70 ^{o}C, and cooled down and placed in a desiccator in order to remove moisture. After that, the hydroxyapatite powders and the dispersant powder were mixed using a 3D shaker mixer (TURBULA ® from WAB company) at different concentrations, as can be seen in Table 3.2 , for thirty minutes. The mixed powders were added incrementally to the resin and thereafter placed in the 3D shaker mixer. After mixing, the resin was ready to be printed.

It is noteworthy that this procedure must be carried out in a radiation free environment so that resin polymerization does not occur.

3.3 3D printing

DLP printer was used to print the pieces from files that were previously modelled using CAD software. Digital Light Processing (DLP) is a process that arises from stereolithography using UV photopolymerised materials. A vat of liquid polymer, constituted by monomers, oligomers, photoinitiators [112] and ceramic powders, is exposed to light from a DLP projector under safelight conditions and the projector displays the image of the 3D model onto the liquid polymer (Figure 3.1). After the layer polymerization, the build platform goes up in order to allow the resin to spread and descends for a height equivalent to the height of the previous one plus the layer thickness, and

Table 3.2: Composition of the different printable suspensions using 0.5 wt% and 2.0 wt% of SDS.

Formulations				
Formulation	HA powder	HA (w/v %)	Dispersant	Dispersant (wt %)
HA1_40_05	HA1	40	SDS	0.5
HA1_40_2	HA1	40	SDS	2.0
HA1_45_05	HA1	45	SDS	0.5
HA2_35_05	HA2	35	SDS	0.5
HA3_45_05	HA3	45	SDS	0.5
HA3_50_05	HA3	50	SDS	0.5
HA4_35_05	HA4	35	SDS	0.5

then the polymerization occurs [85]. This process is repeated until the 3D structure is completed. DLP shows high resolution, fast processing and less shrinkage however this process has high costs and the resin is toxic when uncured [113]. The main difference between DLP and SLA is that SLA laser printing projects the UV radiation point by point while DLP projector printer projects the entire layer into the resin.

A partner company provided a low cost LCD DLP 3D printer which have a compact and dedicated design, easy to use and store and has a colorful user-friendly interface with a 2.8 inch touch screen exhibiting the printing process in real-time. The LED emit a UV light with a wavelength of 405 nm and a light source of 25W and show uniform UV light for a prolonged serving time. The 3D printer is allied to an open-source slicing software capable of processing 30-megabyte file in 1 minute and therefore the file can be stored in an USB (Universal Serial Bus) allowing an offline printing. Furthermore, this printer has the ability to filter bad odors and keep the air clean thanks to an activated carbon air purification system which is beneficial to the user's safety.

The software slices the piece's model into several layers with a thickness defined by the user. Parameters such as normal exposure time, off time, bottom exposure time and bottom layers may also be defined by the user. Moreover, this software allows the addition of supports, not only automatically but also manually, in order to attach the piece to the platform so that it does not drift in the reservoir. The number of supports, their location and where they touch the piece are estimated by the software which are dependent of the architecture, orientation and weight of the piece to be printed. The resin vat has a thin FEP (fluorinated ethylene propylene) film with high quality, high transparency and with a short curing time with a very good curing effect. These features enables the UV light to pass into the resin leading to its cure, the build plate is pulled out, and the cured resin detached from the FEP film.

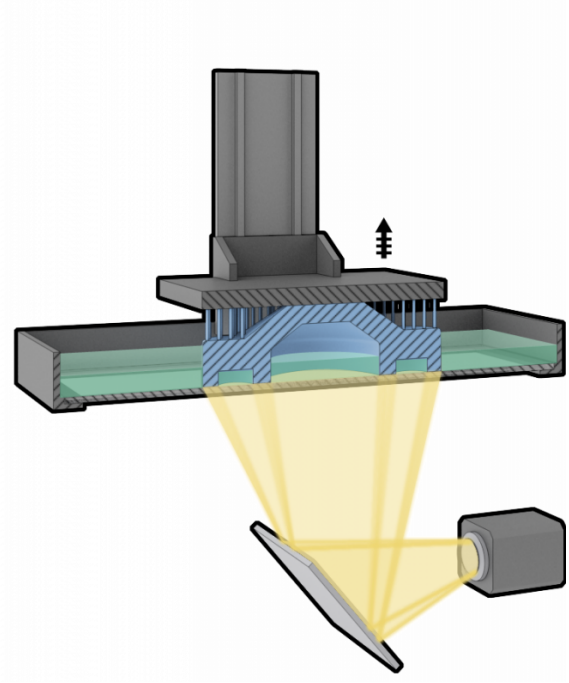

Figure 3.1: Working principle of Digital Light Processing. Adapted from [114].

3.4 Materials characterization

3.4.1 Resin

3.4.1.1 Viscosity measurement

The viscosity of the resin was measured in terms of steady state equilibrium and it was conducted at *Departamento de Engenharia Química*, *Faculdade de Engenharia da Universidade do Porto*. The viscosity was determined with a rotational rheometer MCR92 from Anton Paar supplied with a plate system with a diameter of 50 mm. The test plate is controlled to generate shear rate profiles as a function of the incremental rotational speed. Measurements were performed at 25°C for shear rates in the range of 1-200 s^{-1} and 50 points were acquired to obtain each curve.

3.4.2 Hydroxyapatite powders

3.4.2.1 Granulometric analysis

Granulometric Analysis were obtained at *Departamento de Engenharia Química*, *Faculdade de Engenharia da Universidade do Porto*. The particle size distribution was measured using a COULTER LS 230 laser diffraction analyzer and the powders were suspended in ethanol at 99 %. For the data acquisition, a channel diameter ranged between 0.04-2000 μm and one representative sample of the powder was used for the analysis.

3.4.2.2 Scanning electron microscopy (SEM)

Particle size and shape of hydroxyapatite powders were analysed by SEM and samples were attached to the aluminium supports with carbon tape and then sputtered, through a *SPI Module Sputter Coater* device at 15 mA over 80 seconds, with a thin film of gold-palladium.

The analysis was carried out at *Centro de Materiais da Universidade do Porto* using a *Quanta 400 FEG ESEM / EDAX Genesis X4M*, which is a high resolution (Schottky) Environmental Scanning Electron Microscope with X-Ray Microanalysis and Electron Backscattered Diffraction analysis.

3.4.2.3 X-ray diffraction (XRD)

To determine the thermal stability of the hydroxyapatite powders, X-ray Diffraction analyses were performed at *Serviço de Caracterização de Materiais (SEMAT)*, *Universidade do Minho*.

The samples were analysed before and after sintering in order to verify if there was a phase transformation from HA to β-TCP or α-TCP. A parallelepiped specimen was 3D printed and sintered at 1300 °C, to reach the maximum coesion and resistance, and this sample was then transformed into powder through an agate mortar.

The acquisition was obtained at 1 second per step, a stepsize of 0.04^{o} with a 2θ range between 5^{o} and 80^{o}.

3.4.3 Formulations

3.4.3.1 Deflocullation analysis

In order to evaluate the optimum concentration of surfactant that leads to the lowest viscosity, flow curves were performed for concentrations of surfactant at 0.0 wt%, 0.5 wt%, 1.0 wt%, 1.5 wt%, 2.0 wt% and 2.5 wt%. All the slurries were constituted by 40 w/v% of HA1 hydroxyapatite. These experiments were conducted at *Departamento de Engenharia Química*, *Faculdade de Engenharia da Universidade do Porto* with a rotational rheometer MCR92 from Anton Paar supplied with a plate system with a diameter of 50 mm. Measurements were performed at 25 °C for shear rates in the range of 1-200 s^{-1} and 50 points were acquired. Through the flow curves, the viscosity of each concentration was withdrawn at a shear rate of 200 s^{-1} [115].

3.4.3.2 Viscosity measurements

The viscosity measurements of the ceramic slurries were performed in the same way as the section 3.4.1.1 at the page 26. The viscosity of the formulation was a fundamental parameter for the 3D printing using DLP, as will be discussed later.

3.4.3.3 Cure depth determination

Among all the printing parameters the exposure time to UV light is probably the most important since it is directly correlated with the cured layer thickness. To find out the exposure time needed

for a certain thickness, a cure depth determination was performed [116]. An UV light with a wavelength of 405 nm was applied to the formulation placed inside of the resin vat at different exposure times. The duration of the exposure time varied between 45s and 195s and 16 points were obtained. Finishing each exposure time, the samples were taken from the vat, cleaned with a solvent and the thickness of the sample was measured with a digital vernier caliper with an accuracy of $\pm$ 0.02 mm.

3.4.4 3D printed pieces

3.4.4.1 Scanning electron microscopy (SEM)

The 3D printed and sintered pieces were submitted to SEM analysis to verify the presence of cracks, delamination and their overall geometry. Samples were attached to the aluminum supports with Araldite® glue, fixed with a carbon conductive adhesive tape and coated with a thin film of gold-palladium. The sputtering was performed through a *SPI Module Sputter Coater* device at 15 mA along 120 seconds and the analysis was made at *Centro de Materiais da Universidade do Porto* using a *Quanta 400 FEG ESEM / EDAX Genesis X4M*.

3.4.4.2 Porosity determinations

Porosity plays an important role in bone scaffolds since it ensures largest surface area relatively to dense scaffolds, which allows having friendly conditions for growth of cells and transport of nutrients. The main objective was to obtain a level of porosity compared to that of the human bone. The following equations were used for porosity determination.

$$\rho\ (g/cm^3) = \frac{Mass\ of\ the\ solid\ (g)}{Volume\ of\ the\ solid\ (cm^3)} \tag{3.1}$$

$$Piece's\ Geometric\ Volume\ (cm^3) = Solid's\ Volume\ (cm^3) + Pore's\ Volume\ (cm^3) \tag{3.2}$$

$$Pores\ (\%) = \frac{Pore's\ Volume\ (cm^3)}{Piece's\ Geometric\ Volume\ (cm^3)\ \cdot\ \rho\ (g/cm^3)} \cdot 100 \tag{3.3}$$

Through Equations 3.1, 3.2, 3.3 it is obtained 3.4.

$$Pores\ (\%) = \left(1 - \frac{Mass\ of\ the\ solid\ (g)}{Piece's\ Geometric\ Volume\ (cm^3)\ \cdot\ \rho\ (g/cm^3)}\right) \cdot 100 \tag{3.4}$$

Knowing that the theoretical density of hydroxyapatite is $\rho = 3.16\ g/cm^3$, and that the mass of each sample was measured after sintering, it is possible to obtain the volume of the solid through

the Equation 3.1. To the piece's geometric volume, measured using a vernier caliper with an accuracy of $\pm$ 0.05 mm, the volume of the solid is withdrawn, obtaining the pore's volume. In this way, and using Equation 3.4 it is estimated the pore's percentage.

3.4.5 Volumetric shrinkage determination

In order to evaluate the volumetric shrinkage of the samples, the dimensions were determined using a vernier caliper with an accuracy of $\pm$ 0.05 mm, before and after sintering. Then, the shrinkage value of each dimension can be calculated according to Equation 3.5.

$$Volumetric\ shrinkage\ (\%) = \frac{Initial\ Dimension\ (cm) - Final\ Dimension\ (cm)}{Initial\ Dimension\ (cm)} \cdot 100 \tag{3.5}$$

3.4.6 Mass loss determination

The mass of each piece was measured, using an analytical balance with an accuracy of $\pm$ 0.0001 g, before and after sintering. The mass loss was calculated resorting to Equation 3.6.

$$Mass\ loss\ (\%) = \frac{Initial\ Mass\ (g) - Final\ Mass\ (g)}{Initial\ Mass\ (g)} \cdot 100 \tag{3.6}$$

Chapter 4

Modelling and 3D Printing

Any product obtained through a 3D printing technique has to undergo a previous modelling phase. This phase allows the virtual creation of the product through a Computer-aided-design (CAD) software.

The adopted models had their origin in a single initial model, represented in Figure 4.1 and it mimics the bone's trabecular structure. Representative smaller models were obtained from this initial model that were used in each tests that was performed in this work. To obtain such small models, all of them as STL files, the *3D Builder* software from *Microsoft*® was used.

The STL file creation process converts the continuous geometry in the CAD file into small triangles, or coordinates triplet list of x, y and z coordinates and the normal vector to the triangles. Depending on the complexity of the surface, the number of triangles may change [77].

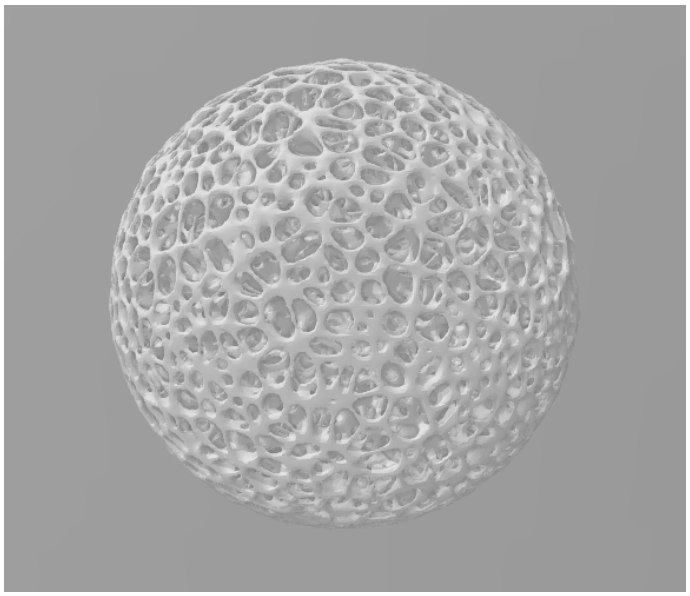

Figure 4.1: Original spherical trabecular model.

3D Builder software allows to rearrange, resize and compile, in order to be able to obtain the desired model. However, the model is not yet printable, as it is necessary to determine the number

of supports and set the 3D printing parameters.

The linkage between the CAD model file and the compatible file for printing was performed through the printer's own software. This is one of the most important steps regarding the 3D printing process.

The input of this software is a STL file where, as said before, will be included supports to the model. The supports are thin cylinders with short tips slightly touching the model that attach the object to the platform and prevent warping (Figure 4.2). These pillars were printed in the same material of the piece and removed manually after printing. The structures have features that can be customized such as the shape of the tip, the radius and the length of the supports, the contact depth and the support angle between the support and the object, and also the structure (light, medium or heavy). The algorithm determines the number of the supports to add according with the defined features and their proper location.

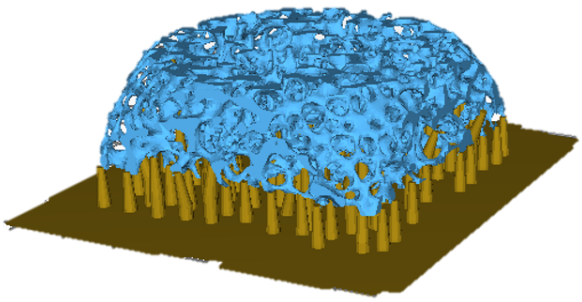

Figure 4.2: Piece's model with the generated supports. In blue is represented the piece and in dark yellow the supports.

Printer parameters are the most important process variables since they affect directly the quality of the printed pieces. These variables are enumerated below:

1. **Layer Thickness (mm)**: Layer thickness reside in the layer height of the slurry that will be polymerized. Low thicknesses are associated to higher resolution while high thicknesses are related with enhanced mechanical properties.

2. **Normal Exposure Time (s)**: Time of exposure to the UV-LED light for each layer. In case the exposure time is too high, the piece loses definition. However, if the exposure is too low the layers will not attach one to each other.

3. **Off Time (s)**: Time interval between the polymerization of consecutive layers. Corresponds to the time that the platform takes to set itself in the next position to polymerize the next layer, and in this way, the resin spreads through all the vat uniformly. The higher the viscosity of the suspension, the higher must be the off time.

4. **Bottom Exposure Time (s)**: Time of exposure to the UV-LED light of each bottom layer.

5. **Bottom Layers**: Number of layers to be polymerized.

It is important to emphasize that increasing the printing parameters may lead to very high printing times. Hence, it is necessary to have an equilibrium between quality and the printing time.

After the parameters have been defined and the supports added, the model was sliced into several layers. This allowed to create paths for the 3D printer to follow when printing, and each path was displayed in the LCD's screen in real time (Figure 4.3). The generated file is compatible with the 3D printer and uploaded to it through a USB stick. The touchscreen enables to choose which file to print, displays the current printing time and the remaining time to finish the printing, the percentage of work already accomplished, the number of layers still to be printed and the cross section of the layer that is being printed. Additionally, the screen allows to stop, pause and continue the printing job during the processing. These are important features since it allowed to stop the printing if something goes wrong, pause the printing to restore the suspension and then continue the printing of the piece.

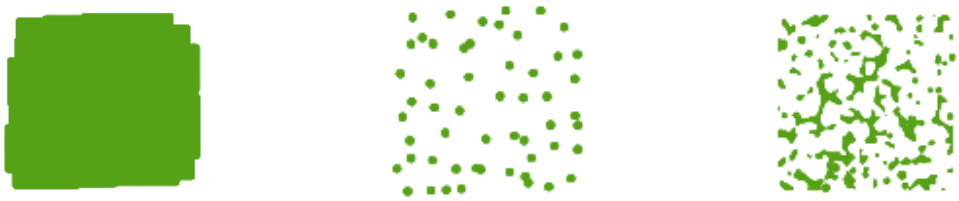

(a) Bottom's Layer (b) Support's Layer (c) Piece's Layer

Figure 4.3: Cross sections of the different constituents of the model to print.

4.1 3D printed models

Starting from Figure 4.1 were created new models (Figure 4.4), whose purposes are different.

The first model (Figure 4.4a) was created in order to carry out the preliminary studies and to define printing parameters. In order to perform the SEM analysis, smaller models (Figure 4.4b and 4.4d) were created to fit in the SEM support. The difference between them is that the model 2 has an open mesh while model 4 has a closed mesh, similar to the bone. Both of them were used to determine if the printed piece shows cracks or delaminations in the structure, and model 4 was also used for evaluate the volumetric shrinkage, the mass loss and the pore's volume of the piece. Model 3 (Figure 4.4c) was resized and thickened to have dimensions of 3 cm x 3 cm x 3 cm after printing to evaluate the volumetric shrinkage, the mass loss and the pore's volume of the piece.

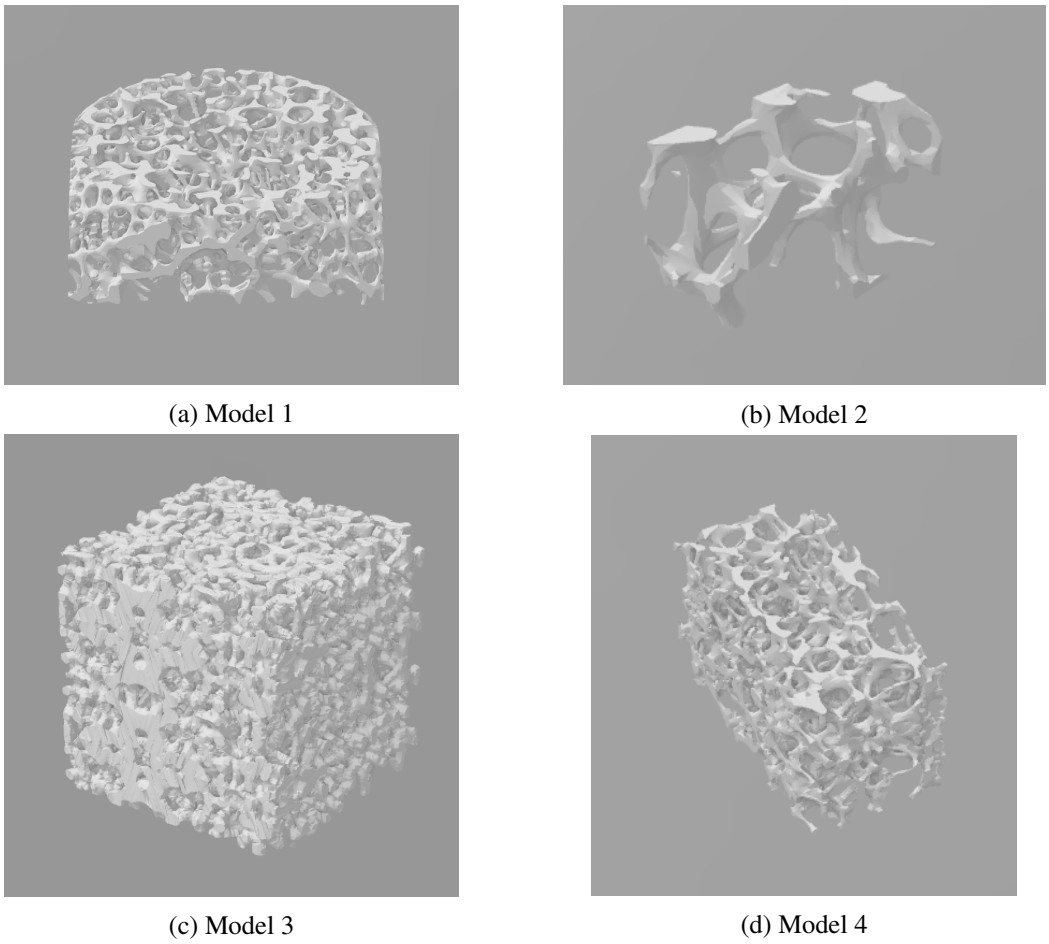

(a) Model 1 (b) Model 2

(c) Model 3 (d) Model 4

Figure 4.4: Different used models created from the original file.

4.2 Post printing procedure

Once the printing was finished, the pieces were carefully removed from the platform using a non-sharp spatula, the resin was filtrated and placed in a container for further use, and both platform and vat were cleaned using isopropyl alcohol, as recommended by resin supplier.

The post-printing is essential to achieve high strength of the 3D printed piece. According to *Johansson et al.* and *Varghese et al.* [111, 117] it was necessary to dive the piece in an appropriate cleaning liquid, in order to ensure that the un-polymerized material was removed. Subsequently, the supports were detached from the piece using a cutting plier and the piece undergone a post-curing treatment. This treatment consists in placing the piece in a UV camera with a wavelength of approximately 400 nm, in order to improve the mechanical properties [118]. Lastly, the samples were subjected to a heat treatment to achieve the desired densification and to improve the mechanical properties. Also, this treatment promotes the photosensitive resin burn-out, leaving behind only the ceramic structure. Figure 4.5 shows this post printing process applied to the Model 1.

Figure 4.6 illustrates the thermal cycle of the ceramic samples. Starting at room temperature, the temperature increases at a heating rate of 0.5 ^{o}C/min until reach the 700^{o}C, temperature at

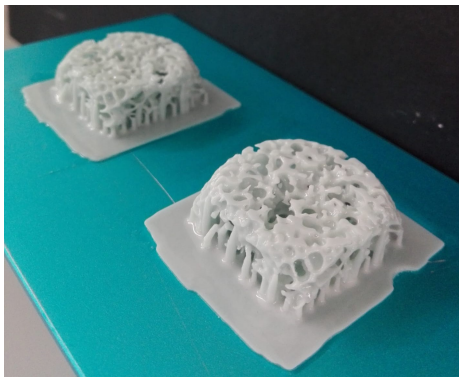

(a) Finished printed piece.

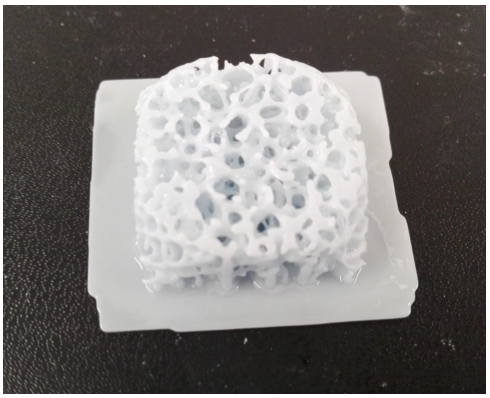

(b) Post-cleaning piece.

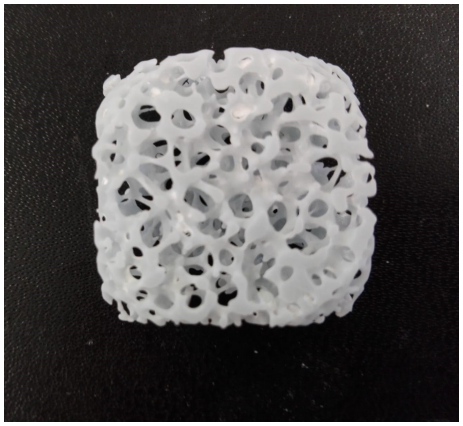

(c) Post removal supports piece.

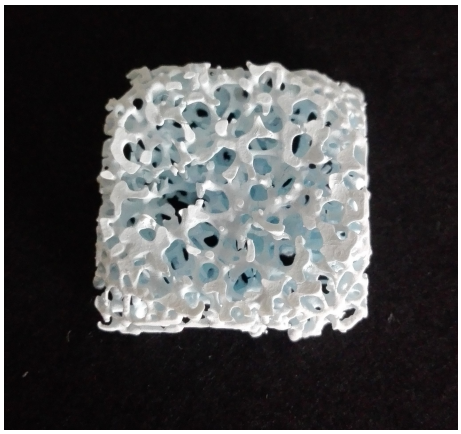

(d) Post-sintering piece.

Figure 4.5: Practical use of the post-printing process applied to Model 1.

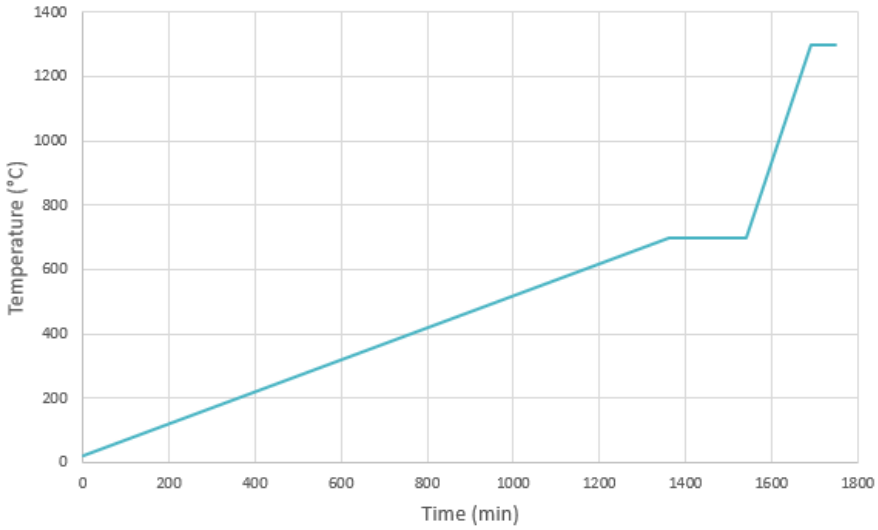

Figure 4.6: Sintering cycle of ceramic samples.

which it remains constant for three hours. These steps allows to remove completely the resin from the structure. Then, the sample is heated to 1300 ^{o}C at a heating rate of 4 ^{o}C/min, and remaining

at this temperature for one hour. As a result, occurs the densification/consolidation of the ceramic particles forming a solid piece. Finally, the piece is allowed to cool down to room temperature inside the furnace.

Chapter 5

Results and Discussion

5.1 Hydroxyapatite powders

The powder morphology and size have influence in the packing density and also in the rheological properties of the suspension such as viscosity, flowability and suspension stability [119]. Therefore the granulometric analysis was performed to evaluate the particle's size distribution using laser diffraction analysis and the particle shape was analyzed resorting to scanning electron microscopy. HA1 hydroxyapatite particles exhibit an uneven particle distribution with a large particle distribution, as can be seen in Figure 5.1a and in the Table 5.1.

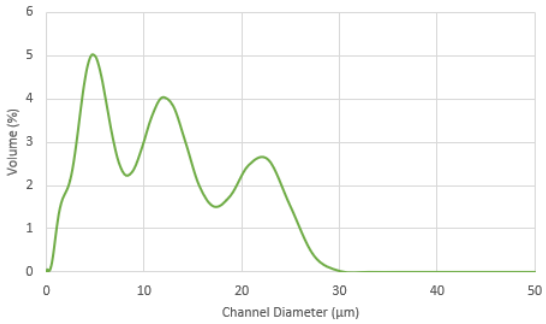

(a) HA1

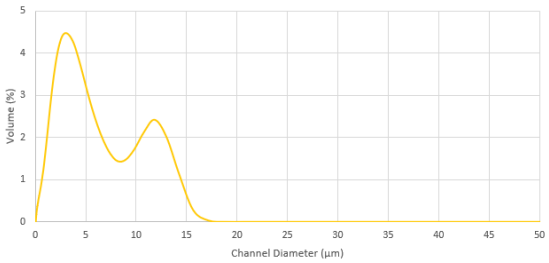

(b) HA2

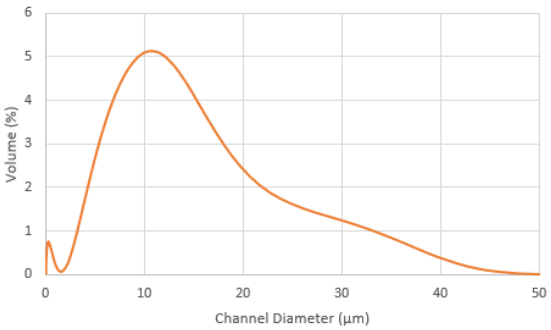

(c) HA3

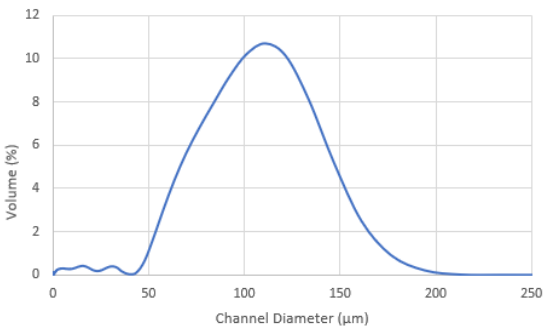

(d) HA4

Figure 5.1: Hydroxyapatite powders granulometric analysis.

Figures 5.2a and 5.3a shows that the HA1 particles are predominantly compact and spherical or with a donut-type format.

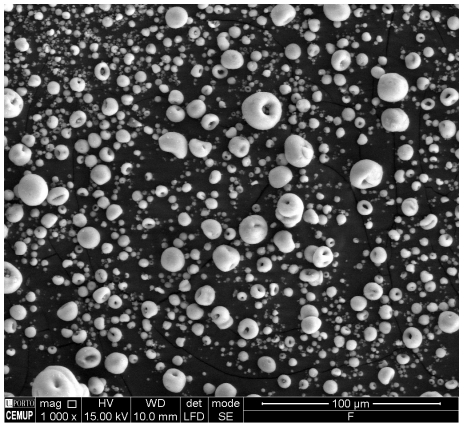

(a) HA1

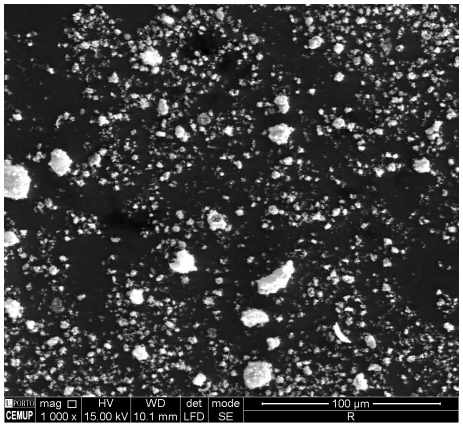

(b) HA2

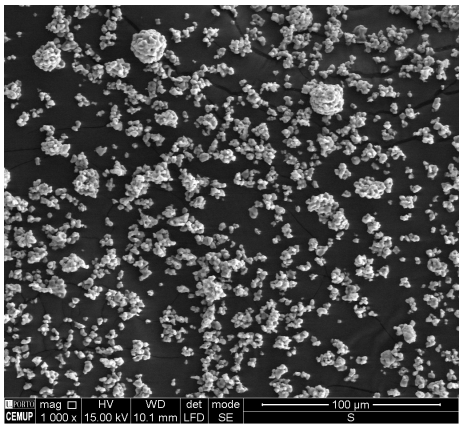

(c) HA3

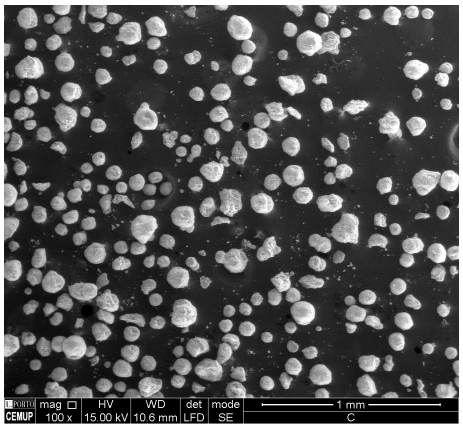

(d) HA4

Figure 5.2: Scanning electron microscopy of the different powders. 5.2a, 5.2b and 5.2c were captured at a magnification of 1000x while 5.2d was captured at a magnification of 100x.

HA2 hydroxyapatite presents a bimodal particle distribution with a smaller particle distribution when compared with HA1 (Figure 5.1b and Table 5.1). However, as can be seen in Figure 5.2b, the particles are floc-type shaped and exhibit high heterogeneity, but at higher magnifications it is found that each particle is composed by an agglomeration of needles (Figure 5.3b).

HA3 also shows a bimodal particle distribution with a large particle distribution (Figure 5.1c) confirmed by the particle size shown in Table 5.1. From Figure 5.2c and Figure 5.3c it is possible to deduce that this is a pre-sintered powder since the grains are in mutual contact. Regarding the shape of the grains, there are a huge divergence between them.

HA4 powder has a unimodal and the highest particle distribution (Figures 5.1d and Table 5.1). Figure 5.2d demonstrates that the particles size of this powder is higher than the others, since this figure has a magnification 10x smaller than all of them. Moreover, it is possible to observe that the particles have different shapes presenting connected crystallites (Figure 5.3d). According to *Chen*

et al. [120] particles with size higher than 10 μm can damage the FEP film of the DLP machine, and since the d_{50} of the HA4 is 99.070 μm, this powder was discarded.

Table 5.1: Particle size of each powder particle using the concept of equivalent spheres. d_{10}, d_{50} and d_{90} corresponds to the percentages 10%, 50%, and 90% of particles under the reported particle size.

	d_{10}	d_{50}	d_{90}
HA1	1.563 μm	5.434 μm	17.470 μm
HA2	0.651 μm	2.878 μm	9.664 μm
HA3	0.338 μm	8.938 μm	21.370 μm
HA4	16.980 μm	99.070 μm	144.9 μm

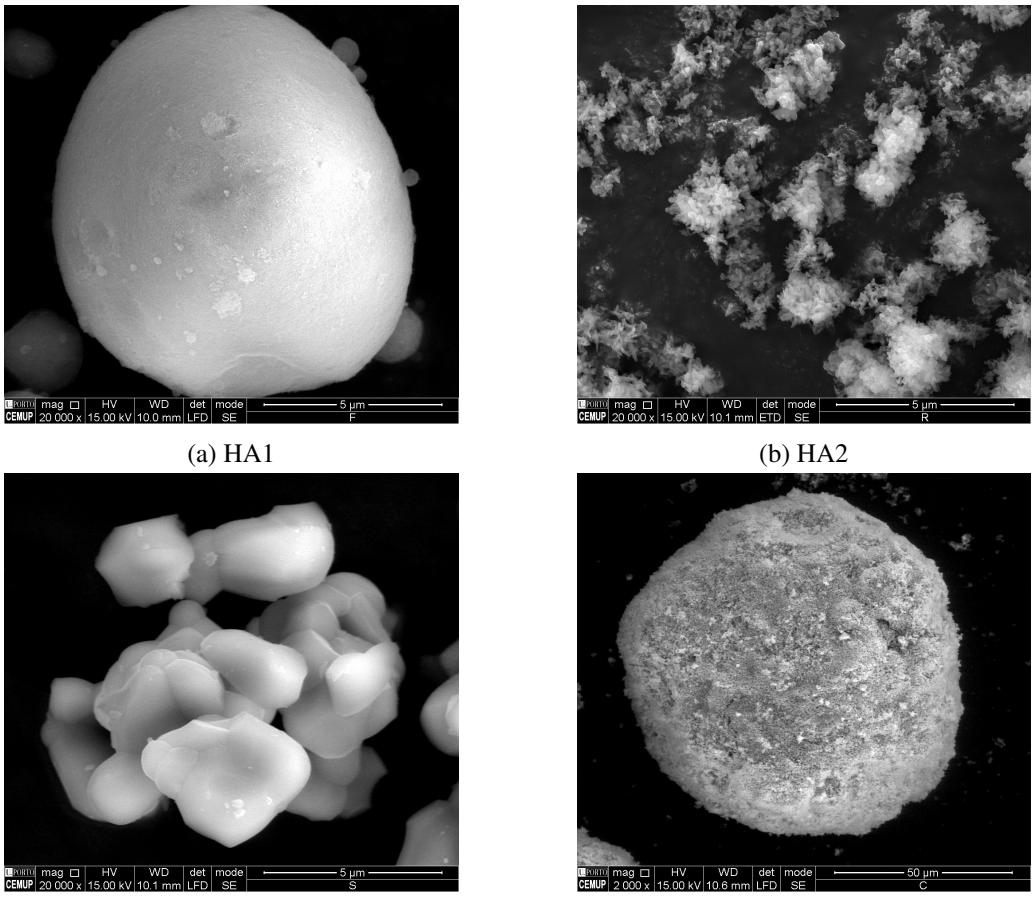

(a) HA1 (b) HA2

(c) HA3 (d) HA4

Figure 5.3: Scanning electron microscopy of the different powders particle. 5.3a, 5.3b and 5.3c were captured at a magnification of 20000x while 5.3d was captured at a magnification of 2000x.

Concerning the identification of crystalline phases present in the powders and thereby the phase composition information, an X-Ray diffraction was performed. In Table 5.2 is summarized

the main intensity peak of possible phases that could be present in this type of materials. To identify the existing phases, the acquired data was compared with the ones of the reference databases. Figure 5.4 represents the diffractogram of the HA1 powder before and after sintering.

Table 5.2: Reference values for the maximum intensity values of the HA and TCP phases. Adapted from [121].

Crystallographic phase	Chemical Formula	2θ value for maximum intensity	ICDD File Card No.
Hydroxyapatite (HA)	$Ca_5(PO_4)_3(OH)$	31.773º	9-432
α-Tricalcium Phosphate (α-TCP)	$Ca_3(PO_4)_2$	30.753º	9-348
β-Tricalcium Phosphate (β-TCP)	$Ca_3(PO_4)_2$	31.025º	9-169

Through the HA1 spectrum (Figure 5.4) it was found that the powder before sintering was poorly crystalline and that after sintering, the powder exhibits crystallinity and a phase transformation occurred in α-TCP and β-TCP. The estimated quantification of these phases is given in percentage in the Table 5.3.

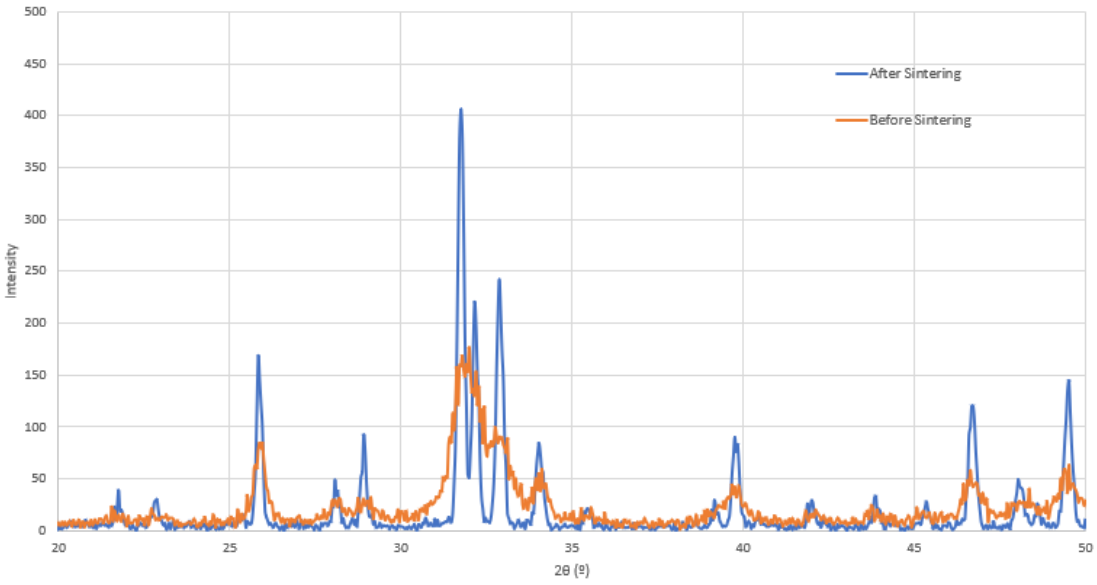

Figure 5.4: HA1 powder diffractogram, before and after sintering.

Looking at the spectrum of HA3, it is verified that before the sintering occurs, it already exhibits crystallinity. This is due to the fact that this powder is already a pre-sintered powder. After sintering, a small phase transformation occurs in β-TCP (Table 5.3). However, as in HA1, these phases have very low intensity peaks relative to the hydroxyapatite peak, so it can be concluded that both powders match to a nearly pure phase of hydroxyapatite.

Table 5.3: Estimated quantification of the crystallographic phases for each powder.

		HA powders			
		HA1		HA3	
		Peak intensity	Phase Percentage	Peak Intensity	Phase Percentage
Chrystallographic phase	HA	406	>98%	418	>97%
	α-TCP	5	-	-	-
	β-TCP	5	-	11	<3%

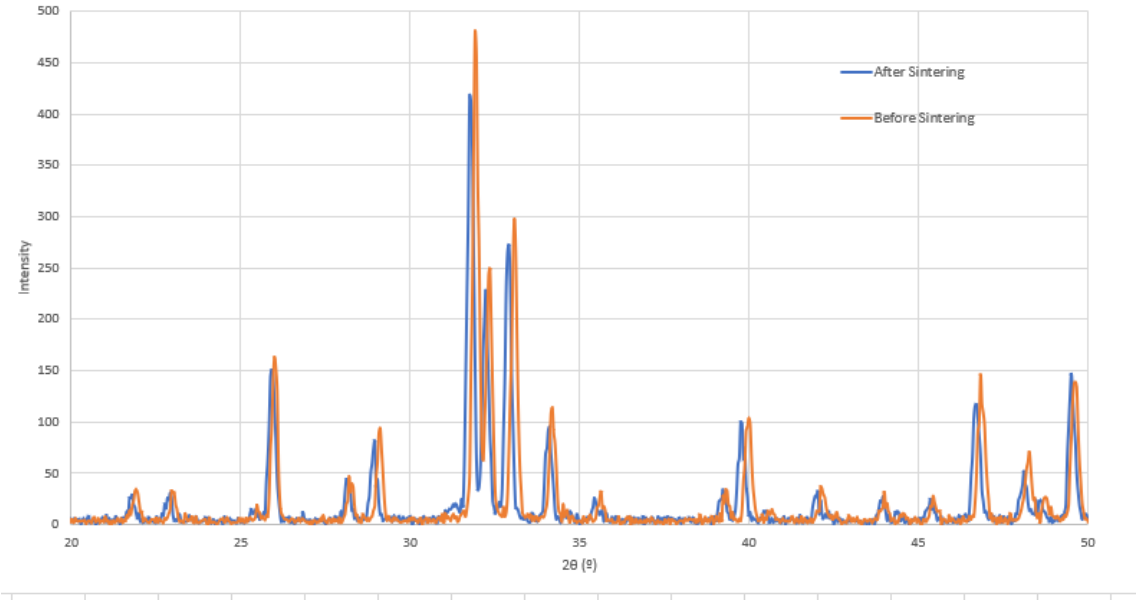

Figure 5.5: HA3 powder diffractogram, before and after sintering.

5.2 Formulations

Ceramic powders have low solubility in polymeric solutions [87] and in order to increase the solubility and the powder dispersion, to have a homogeneous suspension and to make a suspension with high ceramics loading, it is essential to add a dispersant.

Hydroxyapatite have net positive charge. In this contex, the adoption of dispersants with negative charge will result in a deagglomeration of particles by eletrostatic stabilization [122, 123]. Sodium dodecyl sulfate (SDS) was the chosen dispersant based on *Halloran et al.* [124], in which it is advisable to use concentrations between 0.5 wt% and 5.0 wt% for hydroxyapatite suspensions. To find the optimal concentration of dispersant a flocculation curve was performed. Figure 5.6 shows that the concentration with the lowest viscosity is 0 wt% of SDS, however it is mandatory to have a dispersant because they drive the solution stable, decreasing the sedimentation during the 3D printing process.

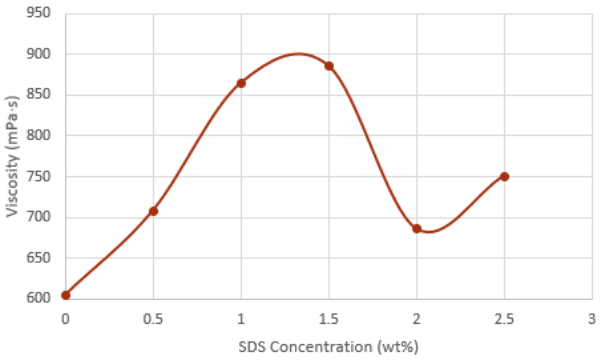

Figure 5.6: Flocculation curve of the suspension with 40 w/v% of HA1 at a shear rate of 200 s^{-1}.

Therefore, 0.5 wt% and 2.0 wt% of SDS were chosen, since these are the concentration values that report lower viscosity. To study whether the dispersant concentration had influence in the formation of cracks and delamination on the 3D printed samples, pieces created with the formulation HA1_40_05 and HA1_40_2 were analyzed by scanning electron microscopy (SEM). It was observed, from the Figure 5.7, that the printed samples with 2.0 wt% of SDS have greater number of cracks compared to those with dispersant concentration of 0.5 wt%. For this reason, the concentration of dispersant was kept constant at a value of 0.5 wt% regarding to the further testing in this work.

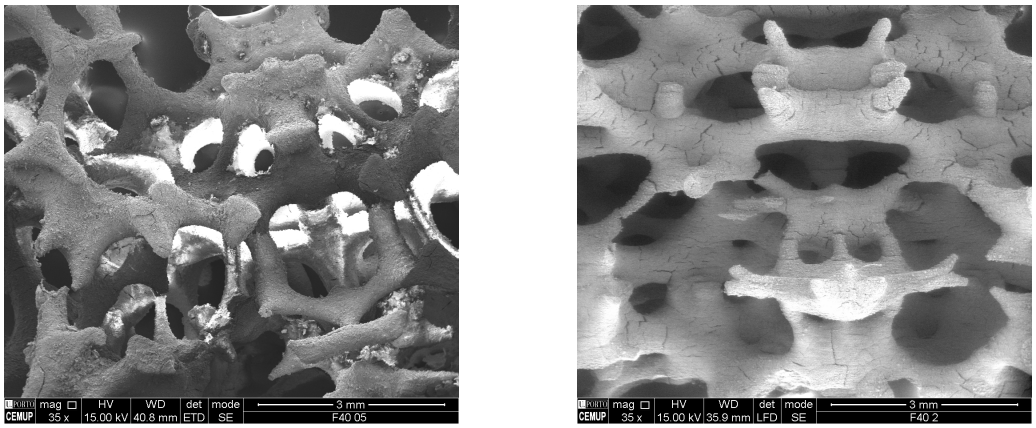

(a) Sample with 0.5 wt% of dispersant concentration. (b) Sample with 2.0 wt% of dispersant concentration.

Figure 5.7: Scanning electron microscopy of the samples with 40 w/v % of hydroxyapatite and different dispersant concentrations. The images were captured at a magnification of 35x.

Viscosity is a crucial factor when studying a suspension behavior.

After determining that the optimum dispersant concentration was 0.5 wt%, it was studied which of the hydroxyapatite powders would originate lowest viscosity. The formulations based on HA4 and HA2 powders were discarded since that the first one has a high sedimentation rate due to having high powder particle size [120] and the second one has very small particles which caused a agglomeration of the suspension due to the fact that this powder presents a particle shape that

deviates from the spherical or equiaxial form [115], and also because the small powder particle size increases the viscosity of the suspension, according to *Chen et al.* and *Konijn et al.* [120, 125].

In this respect, the viscosity's of the different suspensions were measured, as can be seen in Table 5.4 and in Figure 5.8.

Regarding the behavior of the suspensions, all of them exhibit a Newtonian behavior (Figure 5.8), which means that the measured viscosity is independent of the shear rate. Using the same solids loading, 45 w/v%, and the same surfactant concentration, 0.5 wt%, it was found that the suspension with the HA3 powder showed lower viscosity than that of the HA1 (Figure 5.8 and Table 5.4).

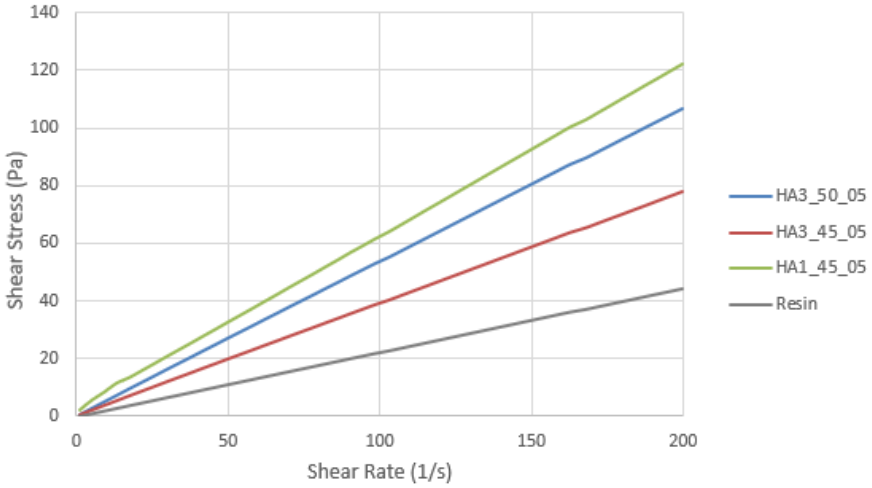

Figure 5.8: Viscosity behavior of the suspensions.

The viscosity values of the suspensions with different solid loadings of HA3 were measured with the aim of determining the behavior of the suspensions with the increase of solid loading. In fact, it is necessary to take into account that the viscosity of the suspensions for the DLP printer should be less than 3 $Pa{\cdot}s$ at 100 s^{-1} according to several works [115, 120, 124, 125, 126, 127]. The obtained results, shown in Table 5.4, have viscosity's below the limit previously exposed which are in agreement with the literature, revealing that with the increase of solid content also increases the viscosity of the suspension, as expected. On the other hand, high solid loads are recommended to avoid formation of fissures, cracks and delamination, to achieve a homogeneous shrinkage during sintering and to obtain dense ceramic pieces [111]. Thus, a balance between viscosity and solids loading should be attained.

Table 5.4: Viscosity values of the different Newtonian suspensions.

Formulation	Viscosity (mPa·s)
Resin	221.6
HA1_45_05	597.3
HA3_45_05	387.9
HA3_50_05	530.6

Formulation HA3_50_05 was used to determine the exposure time needed to reach a certain cured layer thickness. The results are exposed in Figure 5.9 demonstrating that it is possible to determine the exposure time based on the required cured layer thickness for example, if the cured layer thickness chosen is 0.30 mm, the cure time of the suspension must be at least 95s. Initially, the layer thickness increases quickly because of the UV energy absorption by the resin and then the polymerization of the layers occurs in which the formulation is converted from the liquid to the solid state. Also, with the increase of the exposure time, the thickness begins to stabilize since that penetration of UV light becomes difficult due to turbidity of the suspension, which causes less energy to be absorbed by the uncured resin. This effect happens, in the case of our formulation, after 165s of exposure to ultraviolet light, as can be seen in Figure 5.9.

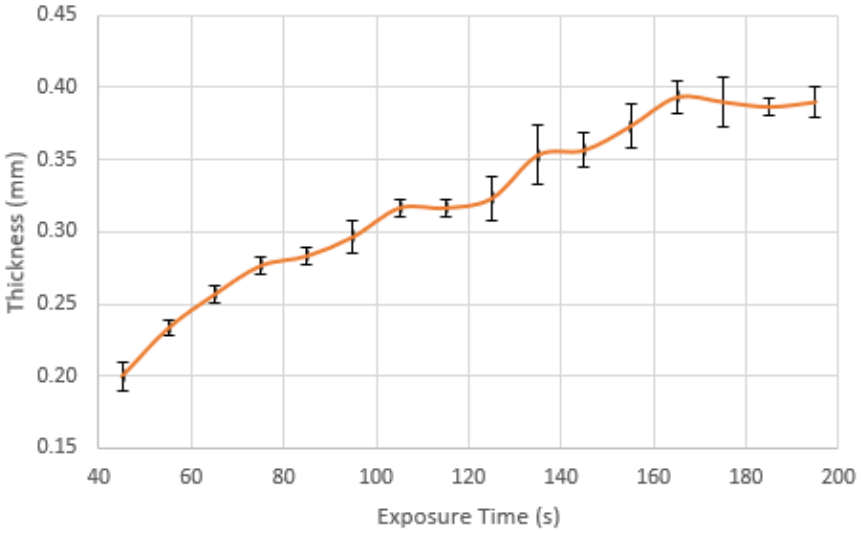

Figure 5.9: Obtained layer thickness with different exposure times and corresponding standard deviations.

5.3 3D printed pieces

The piece's quality can be enhanced with the 3D printing process parameters [128]. The initial parameters used were based upon the user manual and in internet forums. However, in this work novel improved parameters were obtained by trial-error and by using the results obtained in Figure 5.9. The quality of the 3D printed pieces was analysed using a scanning electron microscopy (SEM). The initial parameters would not be sufficient for the layers to adhere well to each other, causing cracks and delamination in the piece (Figure 5.10a). In this way, the layer thickness was decreased in order to have better definition of the build and the normal exposure time was increased to have a better adhesion between layers. Since the suspensions viscosities are low, and that the printing time had to be optimized, the off-time and the bottom exposure time were reduced. However, the number of bottom layers was increased to ensure the necessary supports

so that samples do not fall off on the platform. The optimization of the parameters revealed a decrease in cracks, as can be seen in Figure 5.10b.

The mechanical properties of ceramics may decrease abruptly due to the presence of cracks. Clearly, it is necessary to eradicate all the existing cracks and besides the parameters described above, the cracks may also be caused by the solvent where they are dipped after printing [111]. It was found, through the Figure 5.11, that the S1 promotes cracks and delamination, S3 caused moderate delamination and the S2 is the solvent that causes less delamination and cracks.

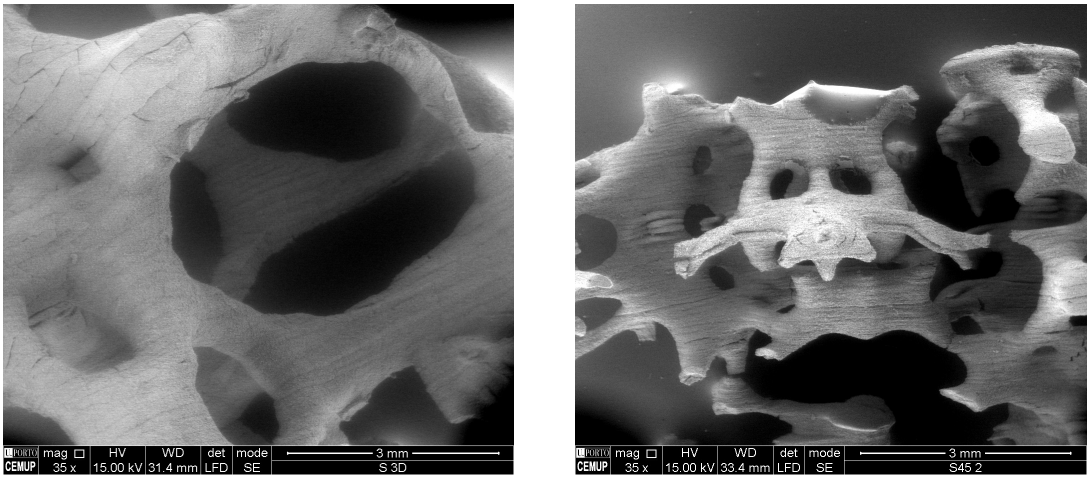

(a) Initial Parameters (b) Optimized Parameters

Figure 5.10: Scanning electron microscopy of the samples printed with HA3_45_05 with different printing parameters. The images were captured at a magnification of 35x.

These solvents were based on a literature survey [111]. These results were only obtained at the end of the dissertation, reason why the pieces produced until then were immersed in solvent S3, since that, according to *Johansson et al.* [111], it was the solvent with the best results. In the future, the solvent with less delamination may be used for cleaning the non-polymerized resin which might be present in the newly 3D printed pieces.

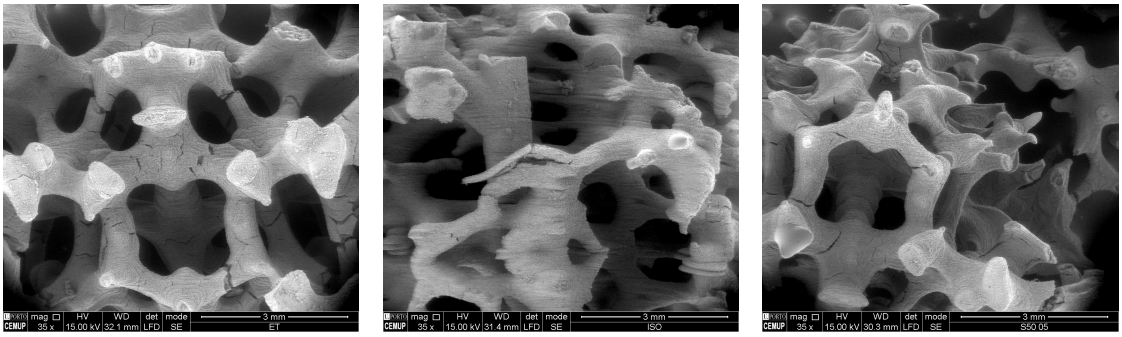

(a) S1 (b) S2 (c) S3

Figure 5.11: Scanning electron microscopy of the samples constituted by 50 w/v% of HA3 and 0.5 wt% with different non-polymerized cleaning liquids. The images were captured at a magnification of 35x.

For the porosity, volumetric shrinkage and mass loss studies, model 3 and 4 were used being obtained through the manipulation of the initial file (Figure 4.1).

One of the noteworthy bone scaffold properties is the porosity, since it improves the bone ingrowth into the scaffolds and encourage osteogenesis [129]. According to the literature, trabecular bone has a porosity between 50% and 90% [130], and similar values can be achieved with the 3D printed scaffolds. The porosity obtained through calculations, indicated in Table 5.5, demonstrate that both models have porosity values close to the human trabecular bone porosity. Model 3 has lower porosity in relation to the model 4, since that in the first model the trabeculae were thickened, which may have caused occlusion of the pores. The increase in solid content showed no influence on the porosity of the piece, however, formulations with powders of different origins were shown to produce pieces with different porosity. This may be due to the viscosity of the formulations since formulations with higher viscosity have less fluidity, which causes the suspension to be trapped between the pores and can be further polymerized.

Table 5.5: 3D printed pieces porosity on Model 3 and 4 with different formulations.

Model	Formulation	Porosity (%)	Standard Deviation (%)
3	HA3_45_05	80.8	0.8
3	HA3_50_05	79.8	0.6
4	HA1_40_05	90.5	0.1
4	HA3_45_05	94.8	0.2
4	HA3_50_05	94.6	0.3

The 3D scaffolds that were fabricated are oriented to be customized according to the patient's defect and therefore it is essential to determine the volume shrinkage percentage for the scaffold to fit perfectly into the bone defect. It was verified that the shrinkage was uneven for the different powders, as can be seen in Table 5.6, being that 3D printed pieces from formulations with HA3 powder reported a smaller shrinkage than the ones with HA1 powder, due to the fact that the first one is already a pre-sintered powder.

Table 5.6: 3D printed pieces volumetric shrinkage on Model 3 and 4 with different formulations.

Model	Formulation	Volumetric Shrinkage (%)	Standard Deviation (%)
3	HA3_45_05	59.2	2.0
3	HA3_50_05	57.7	1.1
4	HA1_40_05	72.9	0.7
4	HA1_45_05	69.8	3.9
4	HA3_45_05	55.4	7.4
4	HA3_50_05	48.9	4.9

It is possible to evidence that increasing the solids loading the shrinkage decreases [131], since the piece printed with HA3_50_05 formulation has lower shrinkage than the piece printed with HA3_45_05 formulation.

The mass loss is a consequence of the burn-out of the resin during the heat treatment. Thus, it is logical that for higher concentrations of hydroxyapatite, the mass loss be lower, which is verified by the values showed in the Table 5.7.

Table 5.7: 3D printed pieces mass loss on Model 3 and 4 with different formulations.

Model	Formulation	Mass Loss (%)	Standard Deviation (%)
3	HA3_45_05	69.9	0.1
3	HA3_50_05	67.0	0.1
4	HA1_40_05	75.6	0.3
4	HA1_45_05	75.3	2.3
4	HA3_45_05	70.4	2.3
4	HA3_50_05	64.0	0.9

Chapter 6

Conclusions and Future Work

Digital light processing technique allowed to sucessfully obtain 3D printed pieces with high solid content and it was capable to reproduce the bone complex microstructure.

Printing parameters decision is vital to the final quality of the 3D printed piece being the most critical parameters the exposure time and the layer thickness. High exposure time led to better adhesion between layers and allowed the piece to not slip off the platform and better resolution was obtained when the layers thickness was decreased. It is worth mentioning that increasing the exposure time and decreasing the thickness of the layers leads to longer printing times, creating printing problems in unstable suspensions.

With the formulation HA3_50_05 the best results have been obtained since it was reached a higher solid content maintaining low viscosity and whose 3D printed pieces produced show very few cracks and delaminations when compared with the other formulations. The medium size powder particles associated with a large and bimodal particle distribution of HA3 powder allowed to achieve low viscosity values which is important to obtain 3D printed pieces with good resolution.

Low surfactant concentrations have been shown to be more effective in reducing viscosity and the cracks than high surfactant concentrations and the high solid loading guaranteed a greater densification of the piece, avoiding the formation of cracks and delamination.

Regarding the formation of cracks and delamination it was found that the resin cleaning solvent has impact in the 3D printed pieces defects. S2 was the solvent who caused less defects and therefore, the one that should be used. The optimized 3D printed pieces showed a porosity similar with that of the bone which is logical since the 3D model was based in a trabecular bone CT scan.

Although there are still work to do, the objective of this dissertation was completely achieved since it was possible to successfully produce, a novel and customizable bone graft not yet available in the market.

As a future work, the stability of HA3_50_05 suspension should be optimized if the printing times are high. Also, further studies applied to a larger number of samples should be carried out on the unpolymerized resin cleaning solvent in order to obtain pieces exempt of cracks and delamination. Moreover, the interaction of the ceramic suspension with different surfactants should

be analysed, to find the surfactant which provides the minimal viscosity in order to be possible to load the resin with a bigger concentration of ceramic powders. Regarding the final 3D printed bone graft, the mechanical properties may be measured, to compare with those of the human bone, and degradation analysis should be performed to check if the material degrades over time. Also, before comercialization of the bone graft here produced, which needs clinical trials, a brief set of experiences to assess their in vitro and in vivo biocompatibility should be performed. Furthermore, it would be insightful to create our own resin in order to reduce production costs and cease to be dependent on suppliers.

References

[1] R. Florencio-Silva, G. R. d. S. Sasso, E. Sasso-Cerri, M. J. Simões, and P. S. Cerri, "Biology of Bone Tissue: Structure, Function, and Factors That Influence Bone Cells.," *BioMed research international*, vol. 2015, p. 421746, jul 2015.

[2] G. Gao, A. F. Schilling, T. Yonezawa, J. Wang, G. Dai, and X. Cui, "Bioactive nanoparticles stimulate bone tissue formation in bioprinted three-dimensional scaffold and human mesenchymal stem cells," *Biotechnology Journal*, vol. 9, pp. 1304–1311, oct 2014.

[3] "Bone Grafting | Johns Hopkins Medicine Health Library," January 2019. Johns Hopkins University School of Medicine, available in https://www.hopkinsmedicine.org/healthlibrary/test{_}procedures/orthopaedic/bone{_}grafting{_}135,316.

[4] V. Campana, G. Milano, E. Pagano, M. Barba, C. Cicione, G. Salonna, W. Lattanzi, and G. Logroscino, "Bone substitutes in orthopaedic surgery: from basic science to clinical practice.," *Journal of materials science. Materials in medicine*, vol. 25, pp. 2445–61, oct 2014.

[5] Grand View Research, "Bone Grafts and Substitutes Market Size, Share & Trends Analysis Report By Material Type (Natural, Synthetic), By Application Type (Spinal Fusion, Craniomaxillofacial, Long Bone), By Region, And Segment Forecasts, 2018 - 2025," tech. rep., Grand View Research, Inc., US, 2018.

[6] F. J. O'Brien, "Biomaterials & scaffolds for tissue engineering," *Materials Today*, vol. 14, pp. 88–95, mar 2011.

[7] G. Turnbull, J. Clarke, F. Picard, P. Riches, L. Jia, F. Han, B. Li, and W. Shu, "3D bioactive composite scaffolds for bone tissue engineering," *Bioactive Materials*, vol. 3, pp. 278–314, sep 2018.

[8] A. S. Brydone, D. Meek, and S. Maclaine, "Bone grafting, orthopaedic biomaterials, and the clinical need for bone engineering," *Proceedings of the Institution of Mechanical Engineers, Part H: Journal of Engineering in Medicine*, vol. 224, pp. 1329–1343, dec 2010.

[9] F. Baino, G. Novajra, and C. Vitale-Brovarone, "Bioceramics and Scaffolds: A Winning Combination for Tissue Engineering.," *Frontiers in bioengineering and biotechnology*, vol. 3, p. 202, 2015.

[10] L. C. Hwa, S. Rajoo, A. M. Noor, N. Ahmad, and M. Uday, "Recent advances in 3D printing of porous ceramics: A review," *Current Opinion in Solid State and Materials Science*, vol. 21, pp. 323–347, dec 2017.

[11] D. Stewart, "3D printing growth accelerates again," 2019. Deloitte, available in https://www2.deloitte.com/insights/us/en/industry/technology/technology-media-and-telecom-predictions/3d-printing-market.html.

[12] D. W. Hutmacher, "Scaffolds in tissue engineering bone and cartilage," *Biomaterials*, vol. 21, pp. 2529–2543, dec 2000.

[13] Office of the Surgeon General, "Bone Health and Osteoporosis," tech. rep., U.S. Department of Health and Human Services, Rockville, 2004.

[14] R. E. Marx and A. K. Garg, "Bone structure, metabolism, and physiology: its impact on dental implantology.," *Implant dentistry*, vol. 7, no. 4, pp. 267–76, 1998.

[15] S. H. Ralston, "Bone structure and metabolism," *Medicine (United Kingdom)*, vol. 45, no. 9, pp. 560–564, 2017.

[16] A. M. Weatherholt, R. K. Fuchs, and S. J. Warden, "Specialized connective tissue: bone, the structural framework of the upper extremity.," *Journal of hand therapy : official journal of the American Society of Hand Therapists*, vol. 25, no. 2, pp. 123–31; quiz 132, 2012.

[17] J. A. Gasser and M. Kneissel, "Bone Physiology and Biology," in *Bone Toxicology* (S. Y. Smith, A. Varela, and R. Samadfam, eds.), ch. 2, pp. 27–94, Basel, Switzerland: Publishing, Springer International, 1 ed., 2017.

[18] K. S. Saladin, *Human Anatomy*. New York, NY: Science Engineering & Math, 5 ed., 2016.

[19] C. VanPutte, J. Regan, R. Seeley, T. Stephens, and P. Tate, *Seeley's Anatomy & Phisiology*. New York: McGraw-Hill Education, 11 ed., 2017.

[20] A. Bassi, J. Gough, M. Zakikhani, and S. Downes, "Bone tissue regeneration," in *Electrospinning for Tissue Regeneration* (L. Bosworth and S. Downes, eds.), ch. 5, pp. 93–110, UK: Woodhead Publishing, 1 ed., 2011.

[21] L. C. Junqueira and J. Carneiro, *Histologia Básica Texto Atlas*. Brazil: NOVA GUANABARA, 12 ed., 2013.

[22] M. B. Schaffler, W.-Y. Cheung, R. Majeska, and O. Kennedy, "Osteocytes: master orchestrators of bone.," *Calcified tissue international*, vol. 94, pp. 5–24, jan 2014.

[23] K. Farbod, M. R. Nejadnik, J. A. Jansen, and S. C. Leeuwenburgh, "Interactions Between Inorganic and Organic Phases in Bone Tissue as a Source of Inspiration for Design of Novel Nanocomposites," *Tissue Engineering Part B: Reviews*, vol. 20, pp. 173–188, apr 2014.

[24] R. Marcus, D. Feldman, D. W. Dempster, M. Luckey, and J. A. Cauley, *Osteoporosis*. USA: Amsterdam : Elsevier/Academic Press, 2013., 4 ed., 2013.

[25] A. C. Guyton and J. E. J. E. Hall, *Textbook of medical physiology*. Philadelphia: Elsevier Saunders, 11th ed., 2006.

[26] S. L. Dallas, M. Prideaux, and L. F. Bonewald, "The Osteocyte: An Endocrine Cell ... and More," *Endocrine Reviews*, vol. 34, pp. 658–690, oct 2013.

[27] R. Oftadeh, M. Perez-Viloria, J. C. Villa-Camacho, A. Vaziri, and A. Nazarian, "Biomechanics and Mechanobiology of Trabecular Bone: A Review," *Journal of Biomechanical Engineering*, vol. 137, p. 15, jan 2015.

[28] C. H. Turner, J. Rho, Y. Takano, T. Y. Tsui, and G. M. Pharr, "The elastic properties of trabecular and cortical bone tissues are similar: results from two microscopic measurement techniques," *Journal of Biomechanics*, vol. 32, pp. 437–441, apr 1999.

[29] S. Bandyopadhyay-Ghosh, "Bone as a Collagen-hydroxyapatite Composite and its Repair," *Trends Biomater. Artif. Organs*, vol. 22, no. 2, pp. 116–124, 2008.

[30] A. D. Pria Bankoff, "Biomechanical Characteristics of the Bone," in *Human Musculoskeletal Biomechanics* (T. Goswani, ed.), ch. 4, p. 244, Brazil: InTech, 1 ed., jan 2012.

[31] S. Pal, *Design of Artificial Human Joints & Organs*. Boston, MA: Springer US, 1 ed., 2014.

[32] M. J. Mirzaali, J. J. Schwiedrzik, S. Thaiwichai, J. P. Best, J. Michler, P. K. Zysset, and U. Wolfram, "Mechanical properties of cortical bone and their relationships with age, gender, composition and microindentation properties in the elderly," *Bone*, vol. 93, pp. 196–211, dec 2016.

[33] P. Zioupos and J. D. Currey, "Changes in the stiffness, strength, and toughness of human cortical bone with age," *Bone*, vol. 22, pp. 57–66, jan 1998.

[34] N. Rucci, "Molecular biology of bone remodelling.," *Clinical cases in mineral and bone metabolism : the official journal of the Italian Society of Osteoporosis, Mineral Metabolism, and Skeletal Diseases*, vol. 5, pp. 49–56, jan 2008.

[35] D. Hadjidakis and I. I. Androulakis, "Bone Remodeling," *Annals of the New York Academy of Sciences*, vol. 1092, pp. 385–396, dec 2006.

[36] J. S. Kenkre and J. Bassett, "The bone remodelling cycle," *Annals of Clinical Biochemistry*, vol. 55, no. 3, p. 20, 2018.

[37] H. Zhou, S. S. Lu, and D. W. Dempster, "Bone Remodeling," in *Osteoporosis in Men* (E. Orwoll, J. Bilezikian, and D. Vanderschueren, eds.), ch. 2, pp. 15–24, USA: Elsevier, 2 ed., 2010.

[38] M. Komoroski, N. Azad, and P. Camacho, "Disorders of bone and bone mineral metabolism," *Handbook of Clinical Neurology*, vol. 120, pp. 865–887, jan 2014.

[39] D. P. Lew and F. A. Waldvogel, "Osteomyelitis," *New England Journal of Medicine*, vol. 336, pp. 999–1007, apr 1997.

[40] T. D. Rachner, S. Khosla, and L. C. Hofbauer, "Osteoporosis: now and the future," *The Lancet*, vol. 377, pp. 1276–1287, apr 2011.

[41] J. A. Kanis, L. J. Melton, C. Christiansen, C. C. Johnston, and N. Khaltaev, "The diagnosis of osteoporosis," *Journal of Bone and Mineral Research*, vol. 9, pp. 1137–1141, dec 2009.

[42] I. Kravets, "Paget's Disease of Bone: Diagnosis and Treatment," *The American Journal of Medicine*, vol. 131, pp. 1298–1303, nov 2018.

[43] D. Tuchendler and M. Bolanowski, "The influence of thyroid dysfunction on bone metabolism.," *Thyroid research*, vol. 7, no. 1, p. 12, 2014.

[44] M. T. Drake, "Osteoporosis and cancer.," *Current osteoporosis reports*, vol. 11, pp. 163–70, sep 2013.

[45] G. M. Bran, J. Stern-Straeter, K. Hörmann, F. Riedel, and U. R. Goessler, "Apoptosis in Bone for Tissue Engineering," *Archives of Medical Research*, vol. 39, pp. 467–482, jul 2008.

[46] R. Dimitriou, E. Jones, D. McGonagle, and P. V. Giannoudis, "Bone regeneration: current concepts and future directions," *BMC Medicine*, vol. 9, p. 66, dec 2011.

[47] P. Kumar, B. Vinitha, and G. Fathima, "Bone grafts in dentistry.," *Journal of pharmacy & bioallied sciences*, vol. 5, p. 4, jun 2013.

[48] S. Gaalen, M. Kruyt, G. Meijer, A. Mistry, A. Mikos, J. van den Beucken, J. Jansen, K. de Groot, R. Cancedda, C. Olivo, M. Yaszemski, and W. Dhert, "Tissue engineering of bone," in *Tissue Engineering* (C. van Blitterswijk, P. Thomsen, A. Lindahl, J. Hubbell, D. F. Williams, R. Cancedda, J. D. de Bruijn, and J. Sohier, eds.), ch. 19, pp. 559–610, USA: Elsevier, 2 ed., 2008.

[49] M. Berube, J. Pickett, C. Leonesio, S. Spitz, S. Kleinedler, N. Durlacher, P. Chipman, D. Fredrick, C. Pratt, S. Iani, C. Granniss, M. A. Miles, D. Conroy, J. Weston, and L. C. Lhowe, *The American Heritage medical dictionary.* US: Houghton Mifflin Co, 2nd ed., 2007.

[50] A. T. and J. C., "Osteoinduction, osteoconduction and osseointegration," *European Spine Journal*, vol. 10, pp. S96–S101, oct 2001.

[51] V. Karageorgiou and D. Kaplan, "Porosity of 3D biomaterial scaffolds and osteogenesis," *Biomaterials*, vol. 26, pp. 5474–5491, sep 2005.

[52] S. Bose, M. Roy, and A. Bandyopadhyay, "Recent advances in bone tissue engineering scaffolds," *Trends in Biotechnology*, vol. 30, pp. 546–554, oct 2012.

[53] S. Wu, X. Liu, K. W. Yeung, C. Liu, and X. Yang, "Biomimetic porous scaffolds for bone tissue engineering," *Materials Science and Engineering: R: Reports*, vol. 80, pp. 1–36, jun 2014.

[54] T. A. Taton, "Boning up on biology," *Nature*, vol. 412, pp. 491–492, aug 2001.

[55] M. Niinomi and M. Nakai, "Titanium-Based Biomaterials for Preventing Stress Shielding between Implant Devices and Bone," *International Journal of Biomaterials*, vol. 2011, no. 0, pp. 1–10, 2011.

[56] W. F. Smith and J. Hashemi, *Foundations of materials science and engineering*. New York, NY: McGraw-Hill, 5th ed., 2010.

[57] L. L. Hench, "Bioceramics: From Concept to Clinic," *Journal of the American Ceramic Society*, vol. 74, no. 7, pp. 1487–1510, 1991.

[58] L. Barnes, I. Cooper, I. Mehdawi, and A. Young, "Antibacterial composite restorative materials for dental applications," in *Biomaterials and Medical Device - Associated Infections* (P. Vallittu, ed.), ch. 9, pp. 199–221, UK: Woodhead Publishing, 1 ed., jan 2015.

[59] X. Zhang, M. Cresswell, X. Zhang, and M. Cresswell, "Calcium Phosphate Materials for Controlled Release Systems," in *Inorganic Controlled Release Technology* (X. Zhang and M. Cresswell, eds.), ch. 6, pp. 161–187, UK: Butterworth-Heinemann, 1 ed., jan 2016.

[60] T. Blokhuis, "Bioresorbable bone graft substitutes," in *Bone Substitute Biomaterials* (K. Mallick, ed.), ch. 4, pp. 80–92, UK: Woodhead Publishing, 1 ed., jan 2014.

[61] V. S. Gshalaev, A. C. Demirchan, M. Marei, Y. Kamary, and R. Moussa, *Hydroxyapatite : synthesis, properties, and applications*. Switzerland: Nova Science Publishers, 1 ed., 2012.

[62] E. Rivera, "Hydroxyapatite-Based Materials: Synthesis and Characterization," in *Biomedical Engineering - Frontiers and Challenges* (R. Fazel-Rezai, ed.), ch. 4, p. 386, Croatia: InTech, 1 ed., aug 2011.

[63] K. Lin and J. Chang, "Structure and properties of hydroxyapatite for biomedical applications," in *Hydroxyapatite (Hap) for Biomedical Applications* (M. Mucalo, ed.), ch. 1, pp. 3–19, UK: Elsevier, 1 ed., 2015.

[64] C. J. Damien and J. R. Parsons, "Bone graft and bone graft substitutes: A review of current technology and applications," *Journal of Applied Biomaterials*, vol. 2, no. 3, pp. 187–208, 1991.

[65] J. Lu, H. Yu, and C. Chen, "Biological properties of calcium phosphate biomaterials for bone repair: a review," *RSC Advances*, vol. 8, no. 4, pp. 2015–2033, 2018.

[66] R. Carrodeguas and S. De Aza, "α-Tricalcium phosphate: Synthesis, properties and biomedical applications," *Acta Biomaterialia*, vol. 7, pp. 3536–3546, oct 2011.

[67] S. Somiya and T. Ohji, "Porous Ceramic Materials," in *Handbook of Advanced Ceramics*, ch. 11.2.2, pp. 1131–1148, USA: Academic Press, 2 ed., jan 2013.

[68] P. Liu and G. Chen, "Fabricating Porous Ceramics," in *Porous Materials* (P. Liu, G. Chen, P. Liu, and G. Chen, eds.), ch. 5, pp. 221–302, USA: Butterworth-Heinemann, 1 ed., jan 2014.

[69] A. Bansiddhi and D. Dunand, "Titanium and NiTi foams for bone replacement," in *Bone Substitute Biomaterials* (K. Mallick, ed.), ch. 7, pp. 142–179, UK: Woodhead Publishing, 1 ed., jan 2014.

[70] A. R. Studart, U. T. Gonzenbach, E. Tervoort, and L. J. Gauckler, "Processing Routes to Macroporous Ceramics: A Review," *Journal of the American Ceramic Society*, vol. 89, pp. 1771–1789, jun 2006.

[71] D. W. Hutmacher, M. Sittinger, and M. V. Risbud, "Scaffold-based tissue engineering: rationale for computer-aided design and solid free-form fabrication systems," *Trends in Biotechnology*, vol. 22, pp. 354–362, jul 2004.

[72] W. Wang and K. W. Yeung, "Bone grafts and biomaterials substitutes for bone defect repair: A review," *Bioactive Materials*, vol. 2, pp. 224–247, dec 2017.

[73] P. A. Webb, "A review of rapid prototyping (RP) techniques in the medical and biomedical sector," *Journal of Medical Engineering & Technology*, vol. 24, pp. 149–153, jan 2000.

[74] S. Lohfeld, V. Barron, and P. E. McHugh, "Biomodels of Bone: A Review," *Annals of Biomedical Engineering*, vol. 33, pp. 1295–1311, oct 2005.

[75] M. Sakin and Y. C. Kiroglu, "3D Printing of Buildings: Construction of the Sustainable Houses of the Future by BIM," *Energy Procedia*, vol. 134, no. 0, pp. 702–711, 2017.

[76] T. Grimm, *User's guide to rapid prototyping.* USA: Society of Manufacturing Engineers, 1 ed., 2004.

[77] K. V. Wong and A. Hernandez, "A Review of Additive Manufacturing," *ISRN Mechanical Engineering*, vol. 2012, pp. 1–10, aug 2012.

[78] S. A. Tofail, E. P. Koumoulos, A. Bandyopadhyay, S. Bose, L. O'Donoghue, and C. Charitidis, "Additive manufacturing: scientific and technological challenges, market uptake and opportunities," *Materials Today*, vol. 21, pp. 22–37, jan 2018.

[79] D. M. Gibbs, M. Vaezi, S. Yang, and R. Oreffo, "Hope versus hype: what can additive manufacturing realistically offer trauma and orthopedic surgery?," *Regenerative Medicine*, vol. 9, pp. 535–549, jul 2014.

[80] A. Zocca, P. Colombo, C. M. Gomes, and J. Günster, "Additive Manufacturing of Ceramics: Issues, Potentialities, and Opportunities," *Journal of the American Ceramic Society*, vol. 98, no. 7, pp. 1983–2001, 2015.

[81] W. Gao, Y. Zhang, D. Ramanujan, K. Ramani, Y. Chen, C. B. Williams, C. C. Wang, Y. C. Shin, S. Zhang, and P. D. Zavattieri, "The status, challenges, and future of additive manufacturing in engineering," *Computer-Aided Design*, vol. 69, pp. 65–89, dec 2015.

[82] L. Yang and H. Miyanaji, "Ceramic Additive Manufacturing: a review of current status and challenges," *Solid Freeform Fabrication 2017: Proceedings of the 28th Annual International*, no. August, pp. 652–679, 2017.

[83] E. Hammel, O.-R. Ighodaro, and O. Okoli, "Processing and properties of advanced porous ceramics: An application based review," *Ceramics International*, vol. 40, pp. 15351–15370, dec 2014.

[84] American Society for Testing and Materials, "ASTM F42/ISO TC 261 Develops Additive Manufacturing Standards."

[85] J. Gardan, "Additive manufacturing technologies: state of the art and trends," *International Journal of Production Research*, vol. 54, no. 10, pp. 3118–3132, 2016.

[86] N. Travitzky, A. Bonet, B. Dermeik, T. Fey, I. Filbert-Demut, L. Schlier, T. Schlordt, and P. Greil, "Additive manufacturing of ceramic-based materials," *Advanced Engineering Materials*, vol. 16, no. 6, pp. 729–754, 2014.

[87] A. Bandyopadhyay, S. Bose, and S. Das, "3D printing of biomaterials," *MRS Bulletin*, vol. 40, pp. 108–115, feb 2015.

[88] M. N. Jahangir, M. A. H. Mamun, and M. P. Sealy, "A review of additive manufacturing of magnesium alloys," in *AIP Conference Proceedings* (M. N. Jahangir, M. A. H. Mamun, and M. P. Sealy, eds.), vol. 1980, (Dhaka, Bangladesh), American Institute of Physics Inc., 2018.

[89] Wenbin Li, Amir Ghazanfari, Ming C. Leu and R. G. Landers, "Methods of Extrusion on Demand for High Solids Loading Ceramic," in *Solid Freeform Fabrication Symposium* (Wenbin Li, Amir Ghazanfari, Ming C. Leu and R. G. Landers, eds.), (Austin, Texas), pp. 332–345, 2015.

[90] R. Vaidyanathan, J. Walish, J. L. Lombardi, S. Kasichainula, P. Calvert, and K. C. Cooper, "The extrusion freeforming of functional ceramic prototypes," *JOM*, vol. 52, pp. 34–37, dec 2000.

[91] A. Ghazanfari, W. Li, M. C. Leu, and G. E. Hilmas, "A Novel Extrusion Based Additive Manufacturing Process For Ceramic Parts," in *Additive Manufacturing of Smart Parts with Embedded Sensors for In-Situ Monitoring in Advanced Energy Systems*, no. February 2017, (Austin, Texas), pp. 1510–1529, Solid Freeform Fabrication Symposium, 2016.

[92] I. Gibson, D. Rosen, and B. Stucker, "Directed Energy Deposition Processes," in *Additive Manufacturing Technologies*, pp. 245–268, New York, NY: Springer New York, 2015.

[93] M. Zenou and L. Grainger, "Additive manufacturing of metallic materials," in *Additive Manufacturing* (J. Zhang and Y.-G. Jung, eds.), ch. 3, pp. 53–103, UK: Matthew Deans, 1 ed., jan 2018.

[94] G. P. Halada and C. R. Clayton, "The Intersection of Design, Manufacturing, and Surface Engineering," in *Handbook of Environmental Degradation of Materials* (M. Kutz, ed.), ch. 19, pp. 397–422, UK: William Andrew Publishing, 3 ed., jan 2018.

[95] B. Stevens, Y. Yang, A. Mohandas, B. Stucker, and K. T. Nguyen, "A review of materials, fabrication methods, and strategies used to enhance bone regeneration in engineered bone tissues," *Journal of Biomedical Materials Research Part B: Applied Biomaterials*, vol. 85, pp. 573–582, may 2008.

[96] N. Sclater and N. Chironis, *Mechanisms and mechanical devices sourcebook*. United States of America: The McGraw-Hill Companies,Inc., 5 ed., 2007.

[97] E. Napadensky, "Inkjet 3D Printing," in *The Chemistry of Inkjet Inks* (S. Magdassi, ed.), ch. 13, pp. 255–267, Singapore: WORLD SCIENTIFIC, 1 ed., 2009.

[98] K. Dimic-Misic, A. Karakoc, M. Ozkan, H. Ghufran, T. Maloney, and J. Paltakari, "Flow characteristics of ink-jet inks used for functional printing," *Istrazivanja i projektovanja za privredu*, vol. 13, no. 4, pp. 207–212, 2015.

[99] B. Prasad, *CAD / CAM Robotics and Factories of the Future- Volume II: Automation of Design, Analysis and Manufacturing*. Springer International Publishing, first ed., 2016.

[100] B. Mueller and D. Kochan, "Laminated object manufacturing for rapid tooling and pattern-making in foundry industry," *Computers in Industry*, vol. 39, pp. 47–53, jun 1999.

[101] E. MacDonald and R. Wicker, "Multiprocess 3D printing for increasing component functionality.," *Science (New York, N.Y.)*, vol. 353, p. aaf2093, sep 2016.

[102] R. Trombetta, J. A. Inzana, E. M. Schwarz, S. L. Kates, and H. A. Awad, "3D Printing of Calcium Phosphate Ceramics for Bone Tissue Engineering and Drug Delivery," *Annals of Biomedical Engineering*, vol. 45, no. 1, pp. 23–44, 2017.

[103] Loughborough University, "VAT Photopolymerisation | Additive Manufacturing Research Group | Loughborough University," June 2019. Loughborough University, available in https://www.lboro.ac.uk/research/amrg/about/the7categoriesofadditivemanufacturing/vatphotopolymerisation/.

[104] Loughborough University, "Directed Energy Deposition | Additive Manufacturing Research Group | Loughborough University," June 2019. Loughborough University, available in https://www.lboro.ac.uk/research/amrg/about/the7categoriesofadditivemanufacturing/directedenergydeposition/.

[105] Loughborough University, "Sheet Lamination | Additive Manufacturing Research Group | Loughborough University," June 2019. Loughborough University, available in https://www.lboro.ac.uk/research/amrg/about/the7categoriesofadditivemanufacturing/sheetlamination/.

[106] Loughborough University, "Material Jetting | Additive Manufacturing Research Group | Loughborough University," June 2019. Loughborough University, available in https://www.lboro.ac.uk/research/amrg/about/the7categoriesofadditivemanufacturing/materialjetting/.

[107] Loughborough University, "Powder Bed Fusion | Additive Manufacturing Research Group | Loughborough University," June 2019. Loughborough University, available in https://www.lboro.ac.uk/research/amrg/about/the7categoriesofadditivemanufacturing/powderbedfusion/.

[108] Loughborough University, "Binder Jetting | Additive Manufacturing Research Group | Loughborough University," June 2019. Loughborough University, available in https://www.lboro.ac.uk/research/amrg/about/the7categoriesofadditivemanufacturing/binderjetting.

[109] Loughborough University, "Material Extrusion | Additive Manufacturing Research Group | Loughborough University," June 2019. Loughborough University, available in https://www.lboro.ac.uk/research/amrg/about/the7categoriesofadditivemanufacturing/materialextrusion/.

[110] K. Bialik-Wąs, B. Tyliszczak, A. Sobczak-Kupiec, D. Malina, and M. Piątkowski, "The effect of dispersant concentration on properties of bioceramic particles," *Digest Journal of Nanomaterials and Biostructures*, vol. 7, no. 1, pp. 361–366, 2012.

[111] E. Johansson, O. Lidström, J. Johansson, O. Lyckfeldt, and E. Adolfsson, "Influence of resin composition on the defect formation in alumina manufactured by stereolithography," *Materials*, vol. 10, no. 2, p. 11, 2017.

[112] D. K. Patel, A. H. Sakhaei, M. Layani, B. Zhang, Q. Ge, and S. Magdassi, "Highly Stretchable and UV Curable Elastomers for Digital Light Processing Based 3D Printing," *Advanced Materials*, vol. 29, p. 1606000, apr 2017.

[113] G.-H. Wu and S.-h. Hsu, "Review: Polymeric-Based 3D Printing for Tissue Engineering," *Journal of Medical and Biological Engineering*, vol. 35, pp. 285–292, jun 2015.

[114] MANUFACTURINGGUIDE, "Digital Light Processing, DLP | Find suppliers, processes & material," 2019. Manufacturingguide, available in https://www.manufacturingguide.com/en/digital-light-processing-dlp.

[115] E. Cunningham, N. Dunne, G. Walker, and F. Buchanan, "High-solid-content hydroxyapatite slurry for the production of bone substitute scaffolds," *Proceedings of the Institution of Mechanical Engineers, Part H: Journal of Engineering in Medicine*, vol. 223, no. 6, pp. 727–737, 2015.

[116] Q. Huang and L. Guo, "Grind/Lap of Ceramics with UV-Bonded Diamond Wheels," in *Handbook of Ceramics Grinding and Polishing* (T. Doi, E. Uhlmann, and I. Marinescu, eds.), ch. 8, pp. 360–393, William Andrew Publishing, 2 ed., jan 2015.

[117] G. Varghese, M. Moral, M. Castro-García, J. J. López-López, J. R. Marín-Rueda, V. Yagüe-Alcaraz, L. Hernández-Afonso, J. C. Ruiz-Morales, and J. Canales-Vázquez, "Fabrication and characterisation of ceramics via low-cost DLP 3D printing," *Boletín de la Sociedad Española de Cerámica y Vidrio*, vol. 57, pp. 9–18, jan 2018.

[118] G. Salmoria, C. Ahrens, M. Fredel, V. Soldi, and A. Pires, "Stereolithography somos 7110 resin: mechanical behavior and fractography of parts post-cured by different methods," *Polymer Testing*, vol. 24, pp. 157–162, apr 2005.

[119] Malvern Instruments Worldwide, "A basic guide to particle characterization," tech. rep., Malvern Instruments Worldwide, UK, 2015.

[120] Z. Chen, J. Li, C. Liu, Y. Liu, J. Zhu, and C. Lao, "Preparation of high solid loading and low viscosity ceramic slurries for photopolymerization-based 3D printing," *Ceramics International*, vol. 45, pp. 11549–11557, jun 2019.

[121] "ICDD Database Search - ICDD."

[122] N. Monmaturapoj and C. Yatongchai, "Influence of preparation method on hydroxyapatite porous scaffolds," *Bulletin of Materials Science*, vol. 34, pp. 1733–1737, dec 2011.

[123] B. Tyliszczak, A. Sobczak-Kupiec, K. Bialik-Was, and W. Kasprzyk, "Stabilization of ceramics particles with anionic polymeric dispersants.," *Journal of nanoscience and nanotechnology*, vol. 12, pp. 9312–8, dec 2012.

[124] J. W. Halloran, M. Griffith, and T.-M. Chu, "Stereolithography resin for rapid prototyping of ceramics and metals," oct 1997.

[125] B. Konijn, O. Sanderink, and N. Kruyt, "Experimental study of the viscosity of suspensions: Effect of solid fraction, particle size and suspending liquid," *Powder Technology*, vol. 266, pp. 61–69, nov 2014.

[126] D. A. Komissarenko, P. S. Sokolov, A. D. Evstigneeva, I. A. Shmeleva, and A. E. Dosovitsky, "Rheological and Curing Behavior of Acrylate-Based Suspensions for the DLP 3D Printing of Complex Zirconia Parts.," *Materials (Basel, Switzerland)*, vol. 11, p. 11, nov 2018.

[127] K. Li and Z. Zhao, "The effect of the surfactants on the formulation of UV-curable SLA alumina suspension," *Ceramics International*, vol. 43, pp. 4761–4767, apr 2017.

[128] A. Ibrahim and M. Ibrahim, "Optimization of Process Parameter for Digital Light Processing (Dlp) 3D Printing," No. April, (South Korea), pp. 19–22, International Conference on Artificial Intelligence and Soft Computing (ICAISC)At: Seoul, South Korea, 2017.

[129] J. R. Woodard, A. J. Hilldore, S. K. Lan, C. Park, A. W. Morgan, J. A. C. Eurell, S. G. Clark, M. B. Wheeler, R. D. Jamison, and A. J. Wagoner Johnson, "The mechanical properties and osteoconductivity of hydroxyapatite bone scaffolds with multi-scale porosity," *Biomaterials*, vol. 28, pp. 45–54, jan 2007.

[130] A. Vahidgolpayegani, C. Wen, P. Hodgson, and Y. Li, "Production methods and characterization of porous Mg and Mg alloys for biomedical applications," in *Metallic Foam Bone* (C. Wen, ed.), ch. 2, pp. 25–82, Woodhead Publishing, 1 ed., jan 2017.

[131] G. Tarı and J. M. Ferreira, "Influence of solid loading on drying-Shrinkage behaviour of slip cast bodies," *Journal of the European Ceramic Society*, vol. 18, pp. 487–493, may 1998.